DEW Project:
Adelaide Metro Thermal 2022
Project Report
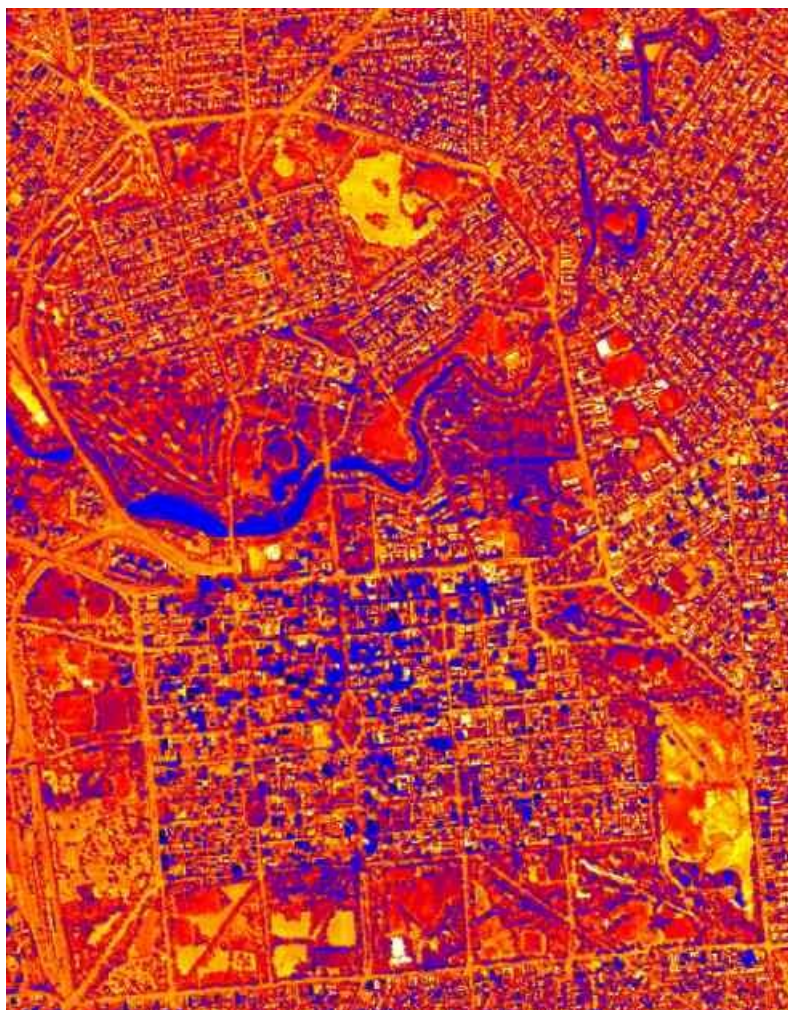
Version 1.0 October 2022

Table of Contents

Introduction

This report details the planning, data collection and processing of a thermal imaging survey of the greater Adelaide metropolitan region, by Airborne Research Australia in March/April 2022 for the South Australian Department of Environment and Water. This project aims at using a thermal imaging camera to map surface temperatures at high resolution in warm to hot conditions, both day and night.

Report by Andrew McGrath, Gustavo Cao Cancio and Caecilia Ewenz.

Data collection by Andrew McGrath, Sharon Drabsch, Grace Gunner and Shakti Chakravarty

Data processing by Andrew McGrath, Marnie Denlay and Grace Gunner

Survey area

The project targets the following area for the study, covering the greater Adelaide metropolitan area from Gawler in the north to Sellicks Beach in the south, and from the coast to the start of the Mount Lofty Ranges..

Illustration 1: Area covered by this project, approximately 90km x 30km in extent with a total area of approximately 1800 km². Shape file provided by DEW with the RFQ.

Instrumentation and equipment

The specified project deliverables are thermal imagery mosaicked, as rasters of surface brightness temperature, a GIS layer of albedo, and geotagged (but not georeferenced) RGB aerial photographs covering the area.

To produce the specified data, ARA used VH-OBS, one of its purpose-built ECO-Dimona aircraft (see "Airborne Platform" below), fitted with the instrumentation shown in Table 1 below.

Table 1: Instruments carried for the study.

Instrument	Model	Purpose	Location
Thermal imager	FLIR A615	Primary science instrument	Outboard underwing pylon (left wing)
DSLR	Canon EOS 5D mk IV, with f/1.2 24mm Canon L2 lens	RGB imagery	Underwing pod (right wing)
Panchromatic linescanner	ARA-developed Runner	Panchromatic imagery for albedo derivation	Underwing pod (left wing)
VNIR hyperspectral linescanner	Specim AISA Eagle-2 (modified)	Hyperspectral imagery, backup for RGB and albedo	Underwing pod (left wing)
INS	OxTS xNav500	Georectification of Eagle and Runner	Underwing pod (left wing)
INS	OxTS RT4003	Georectification of FLIR data	Outboard underwing pylon (left wing)
INS	Novatel SPAN system (LITEF IMU tighly coupled to a Novatel GPS receiver)	Georectification of DSLR images	Underwing pod (right wing)

To obtain data for the precision post-processing of the navigation data, ARA additionally subscribes to the "Hexagon" network of commercially available GNSS base stations, which provides access to several high-quality base stations within the survey area.

To achieve the specified instrument sampling, the aircraft was planned to be flown at a nominal height of 3000m above ground. This gives nominal instrument GSDs as shown in the following table:

Table 2: Instrument imaging parameters.

Instrument	Nominal GSD	Nominal swath
Thermal imager (FLIR)	2 m	1280 m
DSLR	66 cm	4400 m
Runner (albedo)	1 m	2180 m
Eagle	1.9 m	1800 m

A set of parallel, overlapping flight lines with 900m separation ensured full coverage of the required area with a nominal 2m GSD for the thermal imager.

The line density and magnitude of the flight pattern meant that it was expected to require five full survey days to capture the full area. Accordingly, the area was divided into five sub-regions as shown in Illustration 2 below.
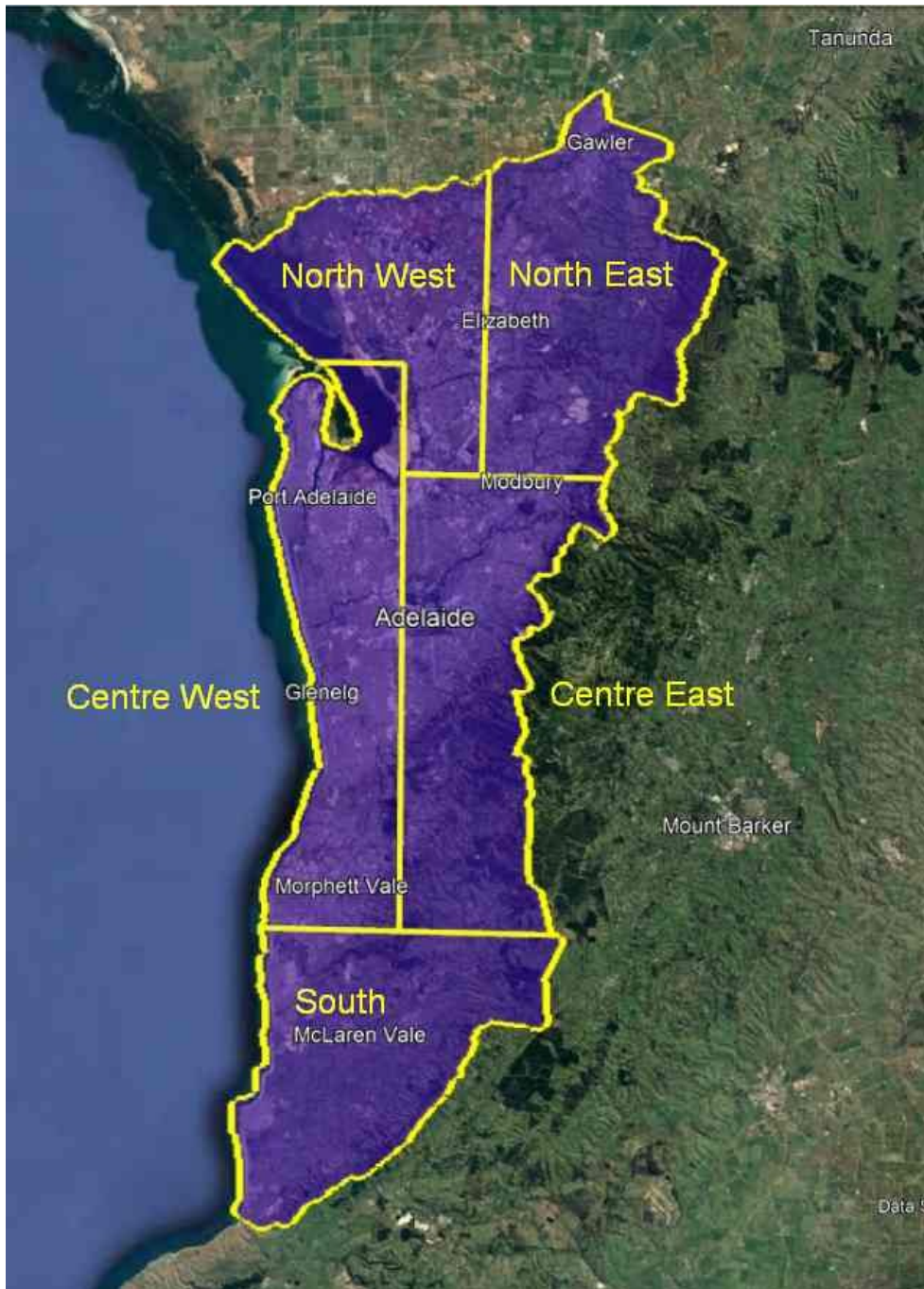
Illustration 2: Division of overall survey region into subregions achievable in a single day/night of flying. Subregion names are shown in yellow.

Details of primary instrumentation

Thermal camera

The thermal camera used for this project is a FLIR model A615 (see appendix for datasheet with full specifications). The camera is controlled via a gigabit ethernet interface using ARA-developed software running on the aircraft's main on-board computer, communicating across the aircraft's local network. The images are time-stamped, and recorded to a solid-state hard drive in the main science computer.

The A615 has a 640 by 480-pixel uncooled micro-bolometer array giving a thermometric resolution of approximately 50mK (one twentieth of a degree C). The camera's internal control electronics monitor the thermal stability of the system and periodically switches a blackbody calibration target into the optical path for a short period (~0.5s) to recalibrate the sensor.

This camera was mounted in a wing-mounted insulated enclosure along with one of the precision navigation units (each instrument mounting location on the aircraft requires its own navigation unit to accurately record the instrument's position and orientation). The thermal stability offered by this insulated enclosure, and by a period of temperature stabilisation flying at a constant altitude before the imaging flight lines (approximately 20 minutes), minimise field-dependent temperature sensing offsets caused by drifts in the physical temperature of the camera (and more particularly, of the embedded detector array).

Instrument settings were controlled by the mission scientist aboard the aircraft during survey via the operating/logging software, will optimise the thermometric resolution, camera focus and data capture rate for the survey conditions.

OxTS RT4003 IMU

As indicated above, a precision navigation unit is also required for each instrument station. There being three instrument stations employed, we used three IMU/GPS systems. Mounted directly with the FLIR thermal imager was an RT-4003 unit from Oxford Technical Solutions (see appendix for full specifications). This unit incorporates a dual-GPS system, accelerometers and gyroscopes to form a full IMU (Inertial Measurement Unit) and was mounted to the same rigid structure as the camera to allow accurate measurement of the position and orientation of the camera.

Before each measurement flight, the IMU/GPS systems were dynamically initialised by taxiing in a straight line at a speed higher than the set threshold speed as set in the configuration of the units (usually 5m/s).

Raw IMU and GPS data were logged internally to the RT4003 unit, allowing the most accurate post-processing analysis to provide the best possible position data.

Airborne Platform

One of ARA's two Diamond Aircraft HK36TTC ECO-Dimonas, VH-OBS, was used as

the airborne platform for the survey. This aircraft type was designed specifically as an environmental sensing platform and on each flight was operated by a pilot and a mission scientist/instrument operator. All of involved pilots not only have considerable expertise in carrying out such operations in complex airspace, but also fully understand the subsequent data processing and interpretation and can therefore factor this knowledge into their considerations and procedures. Most of our mission scientists/instrument operators are also pilots.

The ECO-Dimonas have safety features which are unmatched by standard single-engine survey aircraft, the most relevant of them being their extended glide ration (1:25) in the case of engine failure.

ARA's aircraft are also equipped with live Internet connection at all times, as well as a traffic avoidance system showing the relative position of other aircraft around it on a dedicated display.

<u>Environmental considerations</u>

For any survey, the environmental footprint of the airborne measurements should be taken into account. In this context, such considerations importantly include:

- CO_2-footprint,

- exhaust pollution,

- noise pollution, and

- visual impact.

There is no doubt that the airborne platforms ARA uses for this type of data capture are – by far – the most environmentally friendly platforms of this type available in Australia and even world-wide. In terms of CO_2- and exhaust footprint/pollution, they are unmatched by any other platform (if one excludes electrically driven airborne platforms) due to the modern engine using Premium Unleaded Petrol (PULP) instead of highly leaded Aviation Gasoline (AVGAS). The CO_2-footprint is also closely related to the hourly fuel burn rate of the engine. The typical hourly burn rate for the ECO-Dimona during data capture is approximately 14 litres of PULP, while any other single-engine survey aircraft would have to burn at least 2-3 times this amount of AVGAS. Further, the ECO-Dimonas have no lead in their fuel.

The ECO-Dimonas are also unique in terms of noise pollution. Even flying at 300m AGL, the engine noise is hardly noticeable on the ground, and not at all just a short distance away. Perhaps this impact can be compared to surveys at very low level (20m AMSL and less) over the Great Barrier Reef requiring special permission from the Great Barrier Reef Marine Authority to fly over sensitive areas there which was only granted due to the very low noise footprint of the ECO-Dimona.

Project plan

Based on the area specification above, ARA prepared a flight plan consisting of grids of parallel lines to cover the areas with a 900m line spacing to ensure full overlap of swaths for all instruments. As can be seen in the illustrations below, this required a total of 114 flight lines across the five subregions.

The aircraft endurance is a little over five hours so the subregions were defined to fit within that limitation.

The primary purpose of this study are to investigate the pattern of surface heat distribution across the metropolitan area. This requires that observations be undertaken when the heating mechanisms are similar to those of the most concerning heatwave conditions (dominated by radiation). Both day- and nighttime capture of the area are important, and for comparison purposes the nighttime capture of any part of the area should be made on the night following the matching daytime capture. Meteorological conditions should be consistent with the overall project goals, which mean that the heating pattern should be reprentative of domination by solar heating rather than advected hot air. This means that any survey day and night should ideally have clear skies and low winds throughout the day, and a relatively warm maximum temperature. These requirements can (and did) limit available suitable survey days significantly, given the persistent La Nina conditions bringing higher levels of moisture with consequent cloud, rain and lower temperatures across much of Southern Australia.

Illustration 3: Planned flight lines for northern part of survey area. 24 lines required for the North West subregion, 21 for the North East subregion, 16 for the Centre West, 21 for Centre East, and 32 for the South. This makes a total of 114 flight lines, each to be flown in daytime and nighttime.

Survey activity and Flight reports

18-March – Centre-West subregion

The first data collection flights were undertaken on the 18th of March in good meteorological conditions (clear skies, low winds), taking off a little before local noon for the daytime flight and a little before 11pm for the nighttime. Max BOM-observed temperature at West Terrace was 29.1ºC.
All instrumentation apparently operated without fault for these two ~4-hour flights.

19-March – North-West subregion

The following day also offered good meteorological conditions (clear skies, low winds), again taking off a little before local noon for the daytime flight and a lttle before 11pm for the nighttime. Max BOM-observed temperature at West Terrace was 33.7ºC.

Approximately halfway through the flight, the crew detected a problem with the Runner (panchromatic linescanner, intended for the sensing of albedo) that they thought was resolved by resetting the instrument, and consequently continued the survey but on completion re-flew the approximately half of the survey believed to have been impacted, taking the flight duration for that daytime flight to over five hours. This means that repeat data is available for a large part of the survey area for the other, correctly functioning instrumentation (thermal, RGB and hyperspectral), although for consistency of delivered products, only data from the first overpasses has been incorporated in the processed mosaics.

The nighttime flight was conducted without apparent issue.

26-March – North-East subregion

A period of unsuitable weather following the flights of the 19th delayed the next measurements for a week. These next data collection flights were undertaken on the 26th of March in good meteorological conditions (clear skies, low winds), taking off a little before local noon for the daytime flight and a little before 11pm for the nighttime. Max BOM-observed temperature at West Terrace was 26.5ºC. The following day had warmer conditions forecast but with stronger winds and a forecast of developing cloud. This first pair of flights covered the Centre-West survey sub-region.

All instrumentation apparently operated without fault for these two ~4-hour flights.

15-April – Southern subregion (aborted)

Another period of unsuitable weather following the previous flights led to a more extended delay. A window of two possibly suitable days on the 15th and 16th of April suggested that the South- and Centre-East subregions may be possible, with the weather looking more promising for the 16th. An attempt was made to fly the South subregion on the 15th but convective cloud began to form, casting shadows across the area and disrupting the surface heating patterns. This flight was aborted after covering some 30% of the South subregion, and the data is considered sub-standard because of the cloud shading. Without a suitable daytime data collection, no nighttime flight was attempted.

16-April – Centre-East subregion

The following day's forecast was for significantly better weather, and consequently a pair of flights was made to cover the Centre-East subregion, with the consideration that the advancing season may make this the last good weather oportunity before winter. These next data collection flights were undertaken sucessfully in good meteorological conditions (clear skies, low winds), again taking off a little before local noon for the daytime flight and a little before 11pm for the nighttime. Max BOM-observed temperature at West Terrace was 29.5ºC. The following day had warmer conditions forecast but with stronger winds and a forecast of developing cloud.

This first pair of flights covered the Centre-West survey sub-region.

All instrumentation apparently operated without fault for these two ~4-hour flights.

Southern subregion deferred

An extended period of unsuitable weather followed the flights in mid-April and by the end of the month it was agreed with DEW to defer the final pair of measurement flights until the weather warms up again after winter.

Data processing

It is normal with scientific remote sensing that the total effort is dominated by the data processing and analysis, with the field work being a relatively small component.

Initial data handling

Data processing commenced on the survey day immediately post-flight, with data download, backup and preliminary QA. The volume of data collected for this survey means the data download alone took several hours.

After duplicate off-aircraft raw data backups were complete, the raw data was subject to an initial inspection, and preliminary processing of the recorded navigation data. This showed there to be no fundamental issues such as obvious instrument misbehaviour, navigation problems or environmental issues that reduce data quality.

IMU navigational data processing

Geo-rectification of any of the imagery requires precise knowledge of the location and orientation of the sensor for each raw image collected, and so each instrument is rigidly coupled to an accurate IMU, and the data from these navigation units is processed extremely carefully to achieve the best possible instrument navigation data. This requires substantial post-processing effort, which incorporates data from multiple GPS base stations and precision GPS satellite orbital ephemeris data which is only available one to two weeks after the event. Navigation data processing involved the manufacturer's processing suite (RT-Postprocess from Oxford Technical solutions) with an ARA-modified workflow that incorporates Novatel's Inertial Explorer for the precision post-processing of the GPS component.

The refinement of the measured navigation data to a quality suitable for the georeferencing of the respective remote sensing instruments is essential for accurate georectification of airborne imagery over water. This stage comprises three steps:

1. Acquisition of high precision observed orbital, ionospheric and transmitter clock data. Due to restrictions placed by the operators of the GPS satellite network, these only become available after a waiting period of about two weeks.

2. Post-processing of raw GPS data in NovAtel GrafNav 8.40. Using a combination of high precision auxiliary data, differential processing with the base station data and a number of customised mathematical/physical techniques (e.g. processing under time inversion and back-merging), each individual airborne GPS sample is refined to the highest possible accuracy. The exact quality level achievable at a given time depends on a number of factors (satellite constellation, aircraft orientation, etc.) and varies over time, depending on

satellite orbits, aircraft orientation and flightpath relative to the reference station. For the DEW UHI survey grids, we used data from a base station at Port Stanvac.

3. Merging of the improved GPS fixes with accelerometer and gyro information to yield a consistent high-accuracy, high frequency position/attitude dataset. For the RT units the software package RTpostProcess 111104.14ao was used. The resulting final accuracies again depend on a number of factors - apart from the accuracies of the various input data, in particular the heading drift is significantly influenced by the flight pattern. Long straight sections of flightpath lead to an increased integration error and thus a drift in heading.

During this processing stage, some inconsistencies were detected in the recovered IMU heading values, that impacted the resultant image data georectification accuracies. After extensive analysis and multiple reprocessing explorations over many weeks, this issue was not fully resolved although the heading values have been improved significantly.

Thermal imagery processing

The in-house developed operating and data logging software for the FLIR A615 thermal imager records camera frames as individual files, logged to the aircraft science computer. Based on analysis of the flight plans and imaging parameters for this Adelaide UHI project, the software was configured to record a frame every five seconds, providing >50% nominal forward lap between successive images. Running the imager in this mode for the measurement portion of of each flight, results in several thousand frame files per flight.

Each image is time-tagged by the camera, using an internal crystal counter running at a nominal 2MHz. This time tag is coded into the frame filename for retrieval during processing. The firmware inside the camera delivers each frame as a binary file containing nothing more than the brightness temperature value of each pixel, in units of centi-kelvins coded encoded as unsigned integers. An internal black body calibration target is used to derive a fresh calibration whenever the internal temperature of the camera has drifted beyond limits. Processing of the brightness temperature is therefore a straightforward offset, scaling and type conversion from unsigned integers representing centi-kelvin values, to floating point degrees C.

To produce an orthomosaic of the thermal data, each pixel of each image frame is processed separately in a parametric georectification process rather than by any technique considering correlation of image content. The known collection time of an image is correlated with the high-resolution post-processed navigation data to find the location and orientation of the IMU for that image. Measured as-installed geometric angle offsets between the IMU and the camera's optical axis are applied to obtain the orientation angles for the camera for that frame. A lens calibration conducted in the

laboratory records the x- and y- angle projected by each pixel relative the the camera's optical axis, and thus for each pixel of an image, a ray can be defined in 3-D space, passing through the camera's x/y/z location in the calculated direction. The intersection point of that ray with a DEM identifies the geographic coordinates attributed to that pixel.

ARA's established workflow for applying this georectification process to thermal image frames has been to treat sets of images much like an ensemble of linescan data, working with all images from flight line as a single set, then combining the flight lines at a later stage. However for this project, we found two problems that made this approach problematic. Firstly, the processing time is quite high and the large scale of the project meant processing cycle times of over a week for each iteration through the whole set, where multiple iterations are required to refine the measurements of the angle offsets between the IMU frame-of-reference and that of the camera. Secondly, the issue of heading accuracy from the IMU referred to previously meant that handling many consecutive frames simultaneously in "whole run" subsets didn't give good georeferencing results. As a result, ARA developed a new workflow that handles each frame individually to produce a single geotiff image for each frame, and uses a highly streamlined processing algorithm working with TIN-based DEMs rather than rasters.

The new processing workflow is far superior for the specific characteristics of this project's data, allowing greater processing scope to accommodate a varying heading offset by providing for greater customisation of frame layering when forming the mosaic, and much faster processing times of just a few seconds per frame.

For each of the eight measurement flights, the delivered data includes all individual raw binary frame files, rectified geotiffs of each frame, as well as a single geotiff orthomosaic cropped to the sub-region boundaries.

RGB imagery processing

All individual DSLR image frames were pre-processed using the DxO software for image enhancement/colour optimisation and then the ARA-developed RASP/PPREP/R12 suite used to correlate the individual image frame collection times with the post-processed navigation data from the IMU. This correlation provides the camera location for each image, which was written into a .csv file for each flight, providing approximate latitude, longitude, altitude and orientation angles for each image.

Additionally, these image location data were used with the images in AgiSoft Metashape to derive an orthomosaic for each daytime flight. Please note that, as these mosaics are not a formal project deliverable, only limited effort was put into accurate georeferencing in this process, so the mosaics are cosmetically of high quality but may have significant geometric errors.

Panchromatic imagery processing

The ARA-Runner panchromatic linescanner was carried in order to record panchromatic imagery (400 to 1000nm) for derivation of an albedo layer. It was operated on the daytime flights.

Post-flight, the collected Runner files were QA-checked for number and size of recorded files matching expectations, and for focus and signal levels taking advantage of the available dynamic range. These were then deferred for detailed processing, giving priority to the thermal imagery processing.

Unfortunately, when starting to process the Runner data, it was found that the timing metadata files had somehow been recorded incorrectly and were not usable to georectify the Runner imagery. The precise cause has yet to be investigated, but when it was realised that this data could not be recovered, the Eagle hyperspectral data was used to derive the required albedo layer in its stead.

Hyperspectral data processing

ARA's modified "Eagle-2" hyperspectral linescanner was carried as a backup for the "Runner" panchromatic linescanner for an albedo product, and the Eagle data was originally not planned to be processed. It was operated without problem for all daytime flights. As it turned out, timing problems with the Runner meant that the hyperspectral data was needed to obtain an albedo, and this section describes this processing workflow.

Hyperspectral metadata and run-file organisation

In operation, the Eagle is started logging by the operator at the start of each flight line, and stopped at the end. This results in one large raw data file per run, along with several supporting raw files. These are named automatically by the in-house developed logging software to indicate the time of run start. The metadata file "runs.inc" includes a mapping from these raw filenames to sequentially-allocated run numbers.

 Metadata files describing instrument settings and timing for each flight line, as logged by the instrument operating software, are included with with processed data.

To provide a convenient mechanism to orient a user with the hyperspectral data, we have provided a georeferenced colour-infrared (CIR) representation of each flight line, carrying the same base filename as the gridded hypersepctral reflectance files and at the same spatial resolution. These are in jpeg2000 (.jp2) formate and should load as GIS layers into most GIS tools.

Software used for processing of hyperspectral data

- aisa_radproc – ARA-developed code to implement its own radiometric calibration of its hyperspectral scanners. This program forms an average dark

frame from the raw data file, subtracts that from each image frame and then applies the appropriate calibrated gain frame and non-linearity correction frame to produce an output file in corrected radiometric units. Source code available on request.

- PPREP (Version 1.0) – ARA-developed interpreted text manipulation language processor for preprocessing scripts to either call other software (as identified in this list) directly, or to generate scripts suitable for handling by the other software.

- RASP (Version 0.98) – ARA-developed package of routines for processing airborne remote sensing data.

- GlobalMapper (Versions 12 and 18) – general purpose GIS tool

- ENVI (Version 4, stand-alone licence) – GIS tool well-suited to multi-band processing

- ATCOR4 – industry-standard proprietary code for the atmospheric correction of at-sensor hyperspectral radiances

- AUTO-IT – Windows GUI automation tool able to use scripts to operate GUI-driven software

Overall processing configuration files

Throughout the processing workflow, two overall configuration/control/parameter files are used, named "runs.inc" and "control.inc". Most required parameters are listed in these files, either as definition strings or in look-up tables, using the PPREP syntax. Details about PPREP syntax can be found in the PPREP User Manual available on request.

"control.inc" contains lists of names of files, flightlines, etc. to be processed in the various steps, as well as standard folder names and directory structure information.

"runs.inc" contains mainly look-up tables for specification of runs or flightlines.

Both files are edited manually during processing. These are included in the delivered data disk, and can be found in the "{drive}:\delivery\metadata\processing detail per run" subdirectory.

High level processing flow

- Data backup and archive. Immediately post-flight, two independent, off-aircraft copies are made of all the hyperspectral and navigational data. ARA works with an in-house standardised directory structure for raw data, processed data, and processing scripts. At the outset of processing a hyperspectral dataset, all these directories are set up and populated in accordance with this standard.

- Merging of split raw files (using simple batch file scripts under Windows)

- data entry to tables inside processing script files, to correctly identify all required raw files (using generic text editor)

- radiometric data processing from raw and metadata files to at-sensor radiances (using ARA software PPREP and aisa_radproc)

- geometric processing from post-processed navigation data to IGM files (generating mapping from as-sample geometric format to real-world coordinates, per flight line, using ARA software PPREP and RASP)

- regridding the at-sensor radiances into a regular grid format per flight line, suitable for analysis by ATCOR4 (using ENVI, operated by an AUTO-IT script generated using PPREP)

- Processing of at-sensor radiances to at-surface reflectances (still per flight line, using ATCOR4, operated by an AUTO-IT script generated using PPREP)

Detail of Radiometric Processing

A 'PPREP' script simply invokes aisa_radproc for each raw hyperspectral file, passing as command line parameters the appropriate linearity and gain frames (derived during ARA's own radiometric calibrations). A radiometrically corrected form of the data is then exported in .bsq form.

For each flight line, the new process forms an average dark frame, from the data collected at the end of each the flight line (normally five seconds of data collection with the shutter closed). If the dark frame data for a particular flight line is deemed unsuitable (e.g. in the case of this survey, on several flight lines the shutter did not operate correctly), then dark frame data from a nearby more suitable dark frame collection can be used. This average dark frame is subtracted from each data frame, before dividing by the integration time plus the linearity frame, to get an intermediate frame in units of A-D counts per second. This frame is then scaled by the gain frame to convert to radiometric units.

Georeferencing concept

While it is becoming common practice to use image matching techniques for the orthorectification of frame image data, image correlation does not help with line scan data, and is generally impossible with frame images over a water surface, where the dominant features which may be selected for correlation are likely to be waves on the surface, which of course are moving.

Accordingly, a parametric technique is necessary: for each image (or scan line), the precise location and orientation of the sensor is determined, and then a lens model used to project a ray in 3D space for each pixel in turn. The intersection point of this ray with a known DEM of the target surface then provides the real-world coordinates to be allocated to that pixel.

The location and orientation of the sensor is determined by accurately recording the time of every recorded piece of data, and correlating that with the precision post-processed navigation data from an IMU rigidly mounted with the optics of the imaging sensor. The fixed angles and offsets between the optical axis of the sensor, and the coordinate reference frame of the IMU, (the "Installation Offsets") are added to the navigation data corresponding to the tie of image collection in order to give the sensor position and orientation.

Determination of Installation Offsets

For accurate georeferencing, it is necessary to well-determine the angle offsets between the IMU (and embodied in the post-processed navigation file) and the optical axis of the instruments. This can change small amounts over time, such as between surveys or any time the mechanical installation of the IMU and/or the scanner is disturbed.

Such offset determination is best done by reference to the relative positions of identifiable features in overlapping flight lines. This is most easily done with a re-sampled raster format for the rectified output, since such files are easily opened in correct relationship to each other in a GIS package.

Flight lines are selected for offset determination, based on the availability of clear, ground-based features likely to be visible in overlapping flight lines. Ideally, a geometrical flight pattern will have been flown and scanned – over the runways of the operating airport is commonly selected. Such a pattern normally consists of reciprocal runs in opposite directions along a runway, and a third run crossing that runway at 90 degrees. Data collected over relatively flat, highly structured and well-referenced terrain is also highly appropriate, and for this survey parts of the Adelaide metropolitan area were selected for this purpose. Geotiffs for the calibration flight lines are opened in a GIS tool (ARA uses GlobalMapper for this purpose), and inspected for consistent along- and cross-track offsets between features appearing in the overlapping flight lines flown in different directions. Such offsets are calculated into corrections to the angle offsets currently specified in runs.inc.

This is an iterative process, with the angle offsets progressively refined through a series of georeferencing steps with successively improved offset values.

Precise Georectification

In general for georectification of linescan data, the most accurate DEM available is prepared for the survey area. In the case of this Adelaide metro survey area, SRTM data was used. The RASP scripts for georectification are now adjusted to use this DEM, with output still to geotiff, and these are applied to all runs.

All geotiffs for the survey are opened simultaneously in a GIS tool and carefully inspected for georeferencing issues, run by run. At this stage, survey line numbers are allocated to each flight line, and the run names in runs.inc are updated accordingly.

Production Output of Radiance files

Having reached this stage of processing, the timing and installation offsets have all been determined, and flight lines allocated to survey lines. All data in the 'processed data' directory structure is now deleted, to prevent accidental delivery of product without final processing parameters, and all outputs re-generated using the values now in the runs.inc file. These outputs are:

- Radiometrically corrected files

- Geotiff files

The georectification scripts are now set to output to IGM files (eastings and northings), and the georectification run yet again for all files in the survey. Unfortunately, the header files produced by RASP for BIL/BSQ/BIP formats are not compatible with ENVI and so to facilitate future analysis and inspection of the georeferenced data with ENVI, a stand-alone 'header fix' program is run for each IGM file (i.e. twice per flight line), to modify the headers for ENVI-compatibility.

Production Output of Radiance files

ENVI is able to take a data file in the as-sampled format, along with IGM files defining the eastings and northings for each pixel in that file, and cast the input data into a regular geographic grid of the user's specification. As this is a both GUI-intensive and time-intensive task, and there are many files to be regridded, ARA uses AUTO-IT to apply a GUI-operating script to perform this task for all flight lines. The AUTO-IT script is itself generated using PPREP with the processing parameters defined in the runs.inc file described above.

Atmospheric Correction

With the goal of GIS layers of at-surface spectral reflectances, an atmospheric correction and modelling of incident sunlight provides the expected received radiance from an ideal Lambertian reflector at the surface of unit reflectivity. The ratio of observed radiance to this modelled radiance gives the surface reflectance.

Such application of atmospheric correction requires the selection and/or estimation of a large number of processing parameters, which affect the result in various ways.

Notably:

- ATCOR4 can only process data that has been cast into a regular grid. This has the effect of losing spatial information from the as-sampled format, and requires fixing the spatial resolution of the dataset. Accordingly, before application of the atmospheric correction, all radiance data was resampled onto a 2m grid, as described above.

To provide repeatability and traceability of the processed data, ATCOR4 was invoked for this data using AutoIt scripts.

Albedo layer production

A surface's albedo is the fraction of incident sunlight diffusely reflected from it. As this directly relates to the amount of solar energy resulting in heating of that surface, it is clearly a very important consideration in interpreting or modelling the urban heat island effect.

The hyperspectral at-surface reflectances derived as described above can be integrated across the available spectrum (400 – 1000nm, covering most of the incident solar energy) to form the total fraction reflected across this wavelength range.

Available tools (e.g. ENVI and QGIS) proved not well set up to perform this integration and so a new workflow was developed in R-Studio specifically to do this for each flight line. The output of this process was a set of georeferenced flight line files of albedo, which were overlaid in Global Mapper to form an orthomosaic which was then cropped to the study boundaries.

The resultant albedo layer for the entire survey area is delivered in the "albedo" subdirectory.

Project metadata

Although not a primary project outcome *per se*, the navigation data is provided as metadata supporting the imagery deliverables. For each of the eight measurement flights, a full-resolution .csv file is provided, giving IMU location and orientation as 4ms intervals.

Metadata detailing all flight tracks, including 5-second reports of aircraft altitude and the time-of-day, are provided in the form of KMZ flight track files on the provided data delivery disk. These are all in the directory
   drive:\Nav-metadata
and have names identifying the date and time of the start of the navigation file.

Also provided in the same directory are high temporal resolution (250Hz) .csv files of final-accuracy IMU position and orientation for IMUs supporting both FLIR and Eagle

(warning – these .csv files each have several million lines and conventional spreadsheet programs may not accommodate them conveniently).

Filename	description
220318_002856_rt135_diff_250.kmz	KMZ nav metadata, FLIR, 220318 day
220318_002856_rt135_diff_250.csv	Full (250Hz) nav data, FLIR, 220318 day
220318_112024_rt135_diff_250.kmz	KMZ nav metadata, FLIR, 220318 night
220318_112024_rt135_diff_250.csv	Full (250Hz) nav data, FLIR, 220318 night
220319_004120_rt135_diff_250.kmz	KMZ nav metadata, FLIR, 220319 day
220319_004120_rt135_diff_250.csv	Full (250Hz) nav data, FLIR, 220319 day
220319_114532_rt135_diff_250.kmz	KMZ nav metadata, FLIR, 220319 night
220319_114532_rt135_diff_250.csv	Full (250Hz) nav data, FLIR, 220319 night
220326_000323_rt135_diff_250.kmz	KMZ nav metadata, FLIR, 2203268 day
220326_000323_rt135_diff_250.csv	Full (250Hz) nav data, FLIR, 220326 day
220326_115725_rt135_diff_250.kmz	KMZ nav metadata, FLIR, 220326 night
220326_115725_rt135_diff_250.csv	Full (250Hz) nav data, FLIR, 220326 night
220416_003319_rt135_diff_250.kmz	KMZ nav metadata, FLIR, 220416 day
220416_003319_rt135_diff_250.csv	Full (250Hz) nav data, FLIR, 220416 day
220416_122406_rt135_diff_250.kmz	KMZ nav metadata, FLIR, 220416 night
220416_122406_rt135_diff_250.csv	Full (250Hz) nav data, FLIR, 220416 night

The navigation metadata kmz files described above include the flight tracks themselves, both in 3-D and as a vertically-projected ground track, as well as regular placemarks showing the altitude and the time (in UTC seconds-of-day). If viewed in Google Earth, only the ground track is visible by default on opening, but the other data can be selected on or off by unfolding the KMZ folder structure. The following images show the planned flight lines for each flight, with approximate local time (Australian Central Daylight Time, ACDT) for the middle of each flight line.
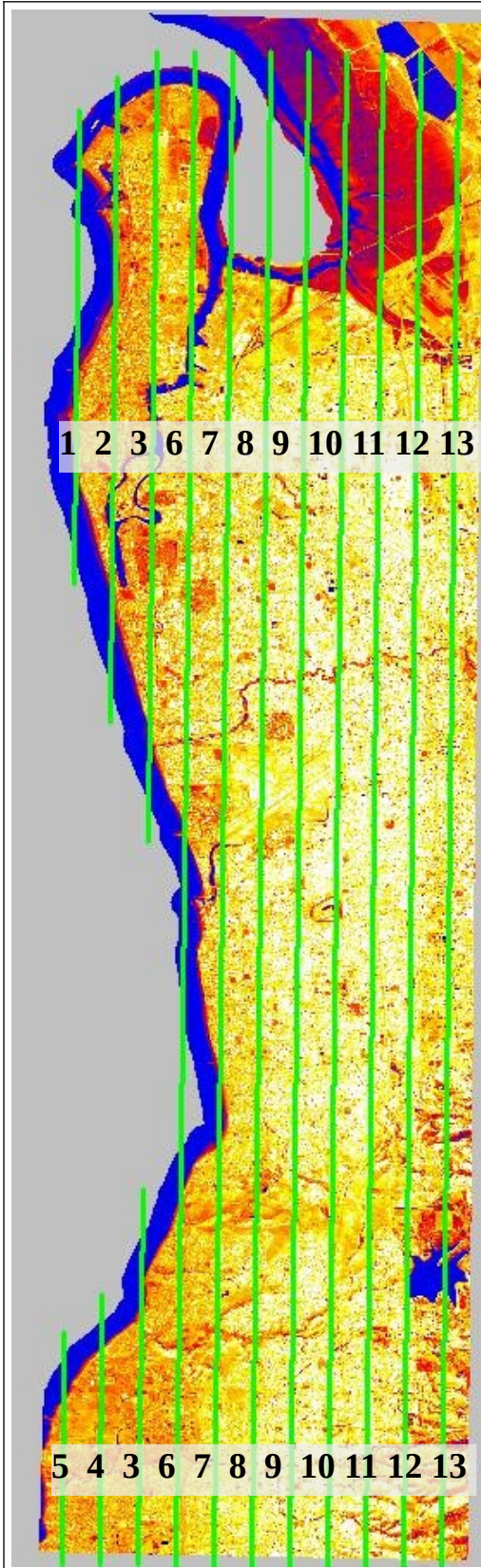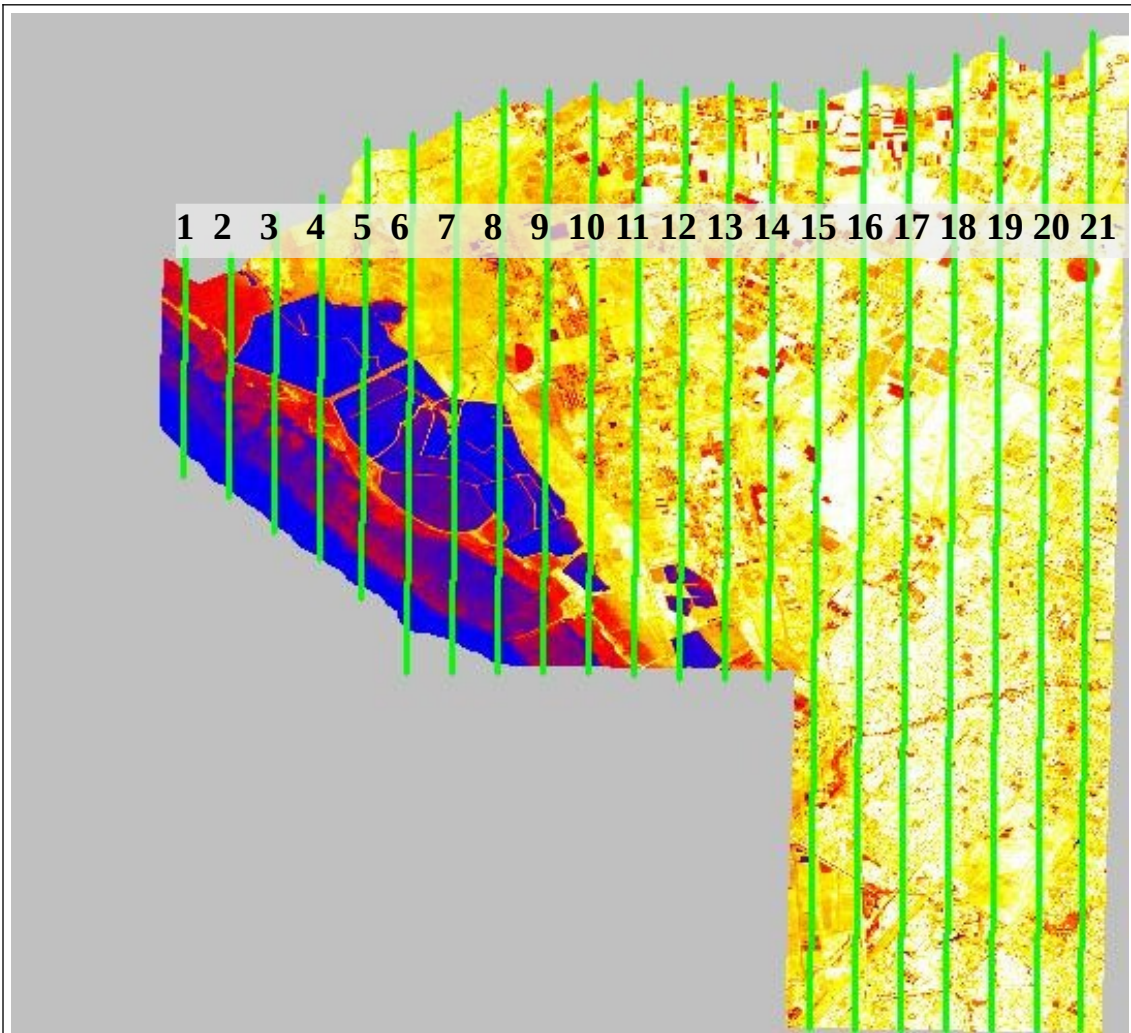
Centre-West daytime (220318) flight line timing

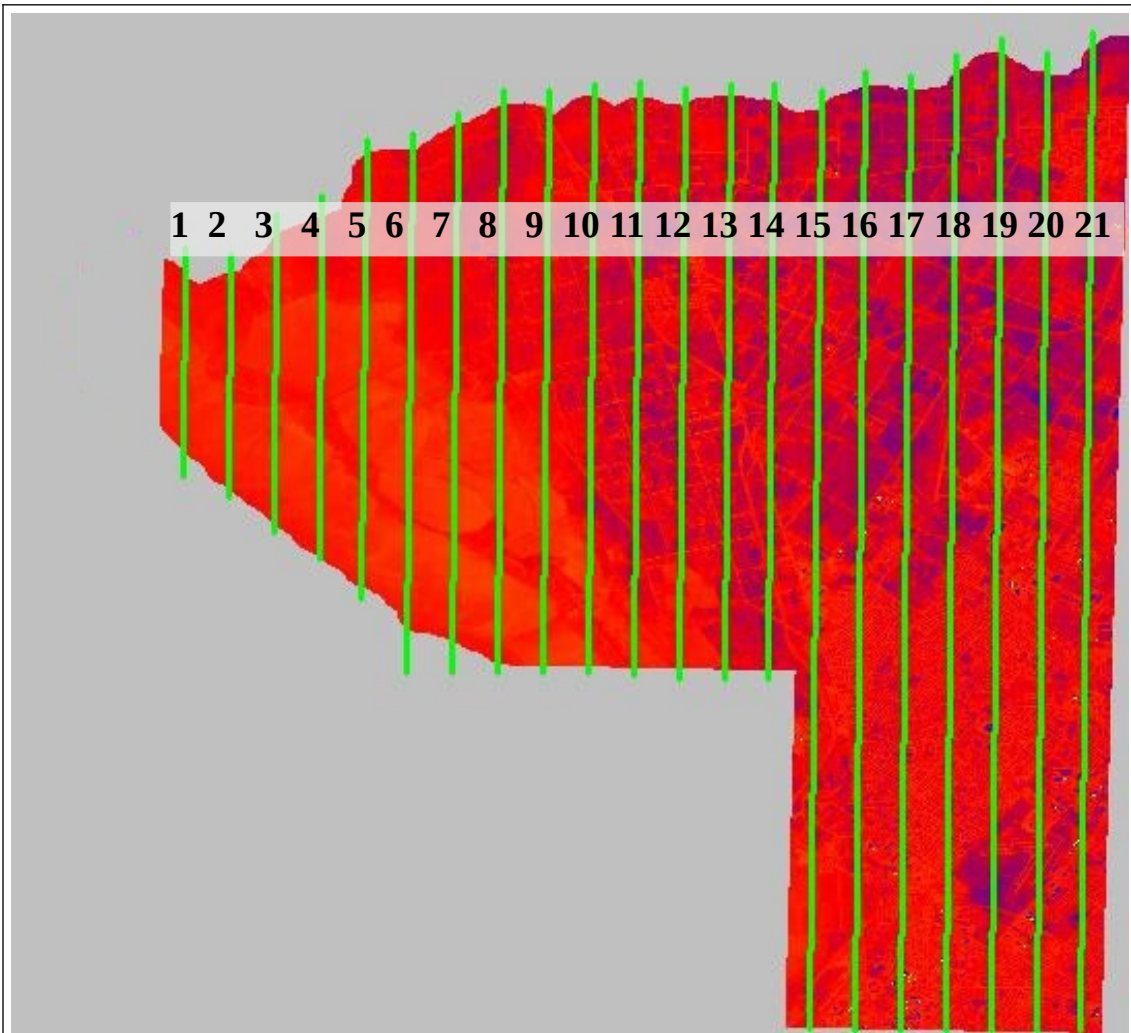| Line number	Mid-point time ACDT
1	12:15
2	12:24
3	12:38
4	12:47
5	12:51
6	13:01
7	13:19
8	13:34
9	13:53
10	14:07
11	14:26
12	14:46
13	15:04
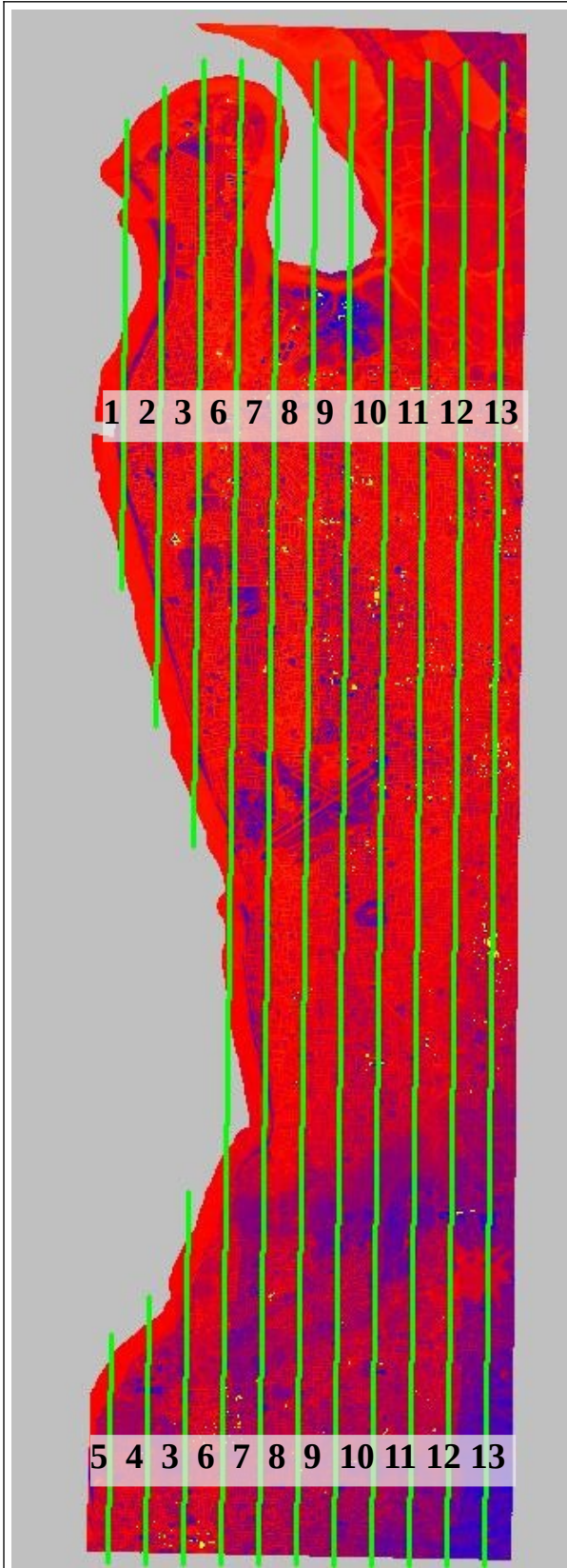
Centre-West nighttime (220318, continuing into the following morning) flight line timing

Line number	Mid-point time ACDT
1	23:01
2	23:05
3	23:17
4	23:30
5	23:33
6	23:46
7	23:59
8	00:19
9	00:32
10	00:52
11	01:08
12	01:29
13	01:41

North-West daytime (220319) flight line timing

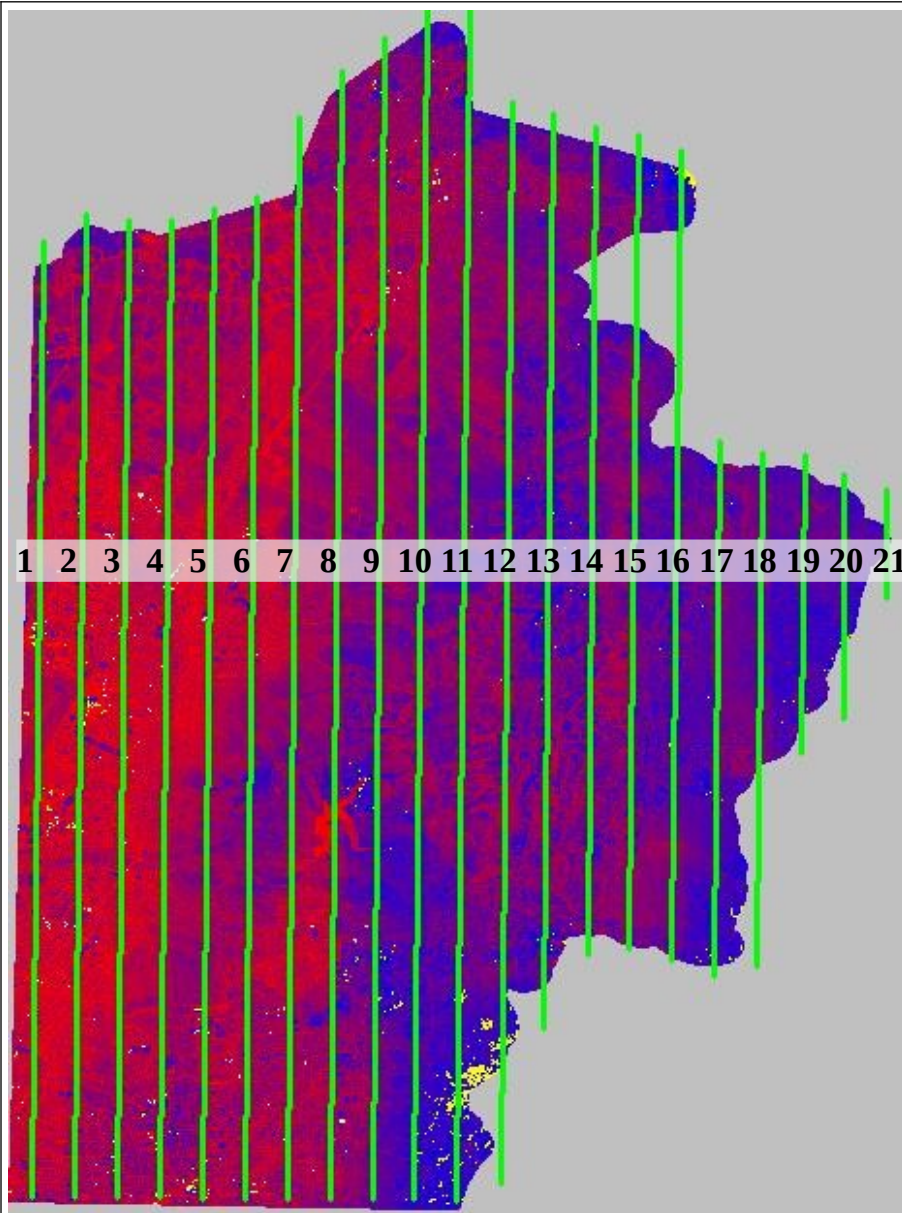| Line number	Mid-point time ACDT		Line number	Mid-point time ACDT
1	12:10		11	13:18
2	12:14		12	13:24
3	12:18		13	13:31
4	12:22		14	13:39
5	12:28		15	13:51
6	12:34		16	14:02
7	12:40		17	14:10
8	12:46		18	14:21
9	12:53		19	14:29
10	12:59		20	14:40
			21	14:49

North-West nighttime (220319, continuing into the following morning) flight line timing

Line number	Mid-point time ACDT		Line number	Mid-point time ACDT
1	23:12		11	00:17
2	23:16		12	00:25
3	23:20		13	00:34
4	23:26		14	00:42
5	23:31		15	00:51
6	23:38		16	01:05
7	23:45		17	01:14
8	23:53		18	01:28
9	00:00		19	01:37
10	00:09		20	01:51
			21	01:59
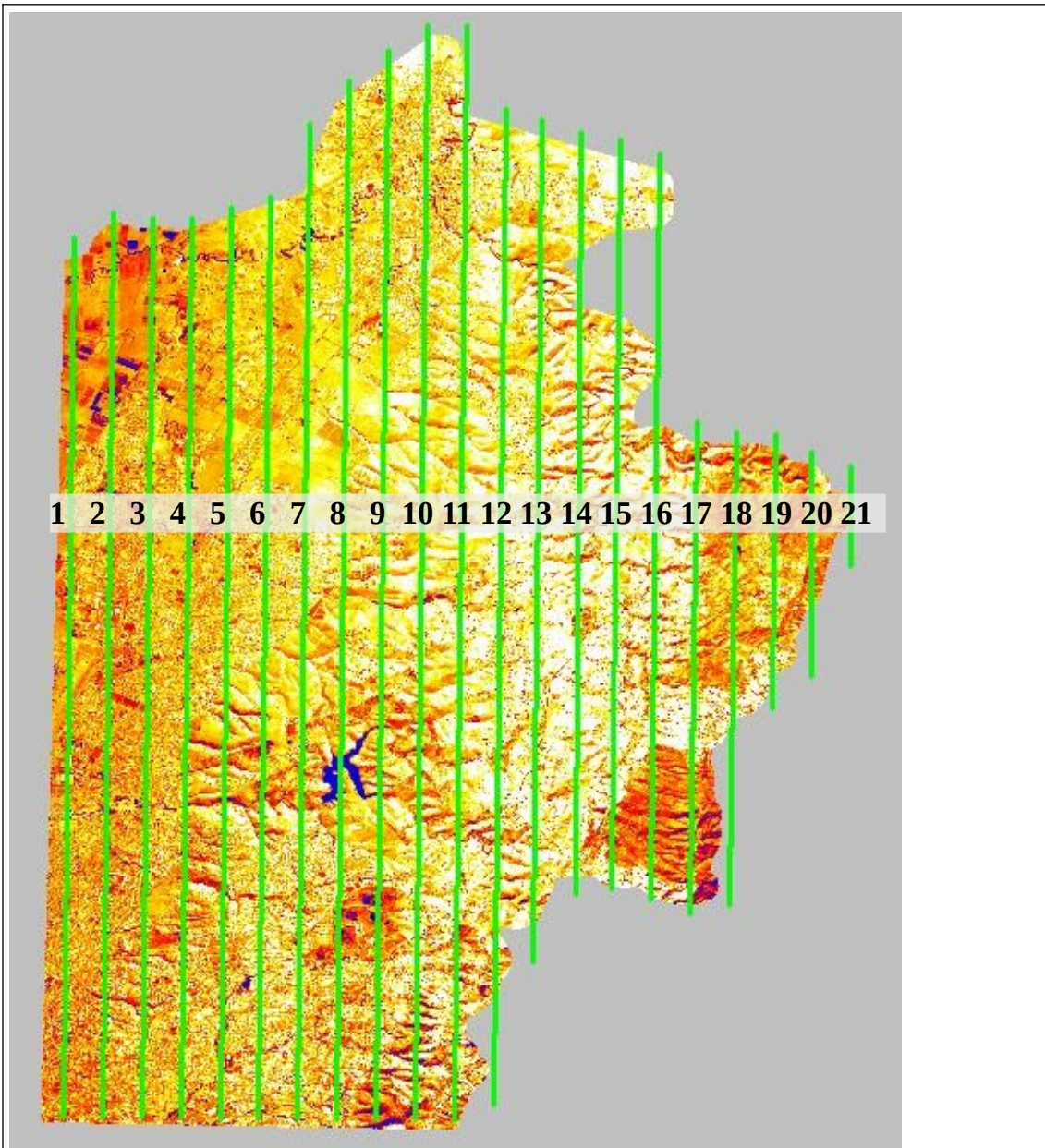
North-East daytime (220326) flight line timing

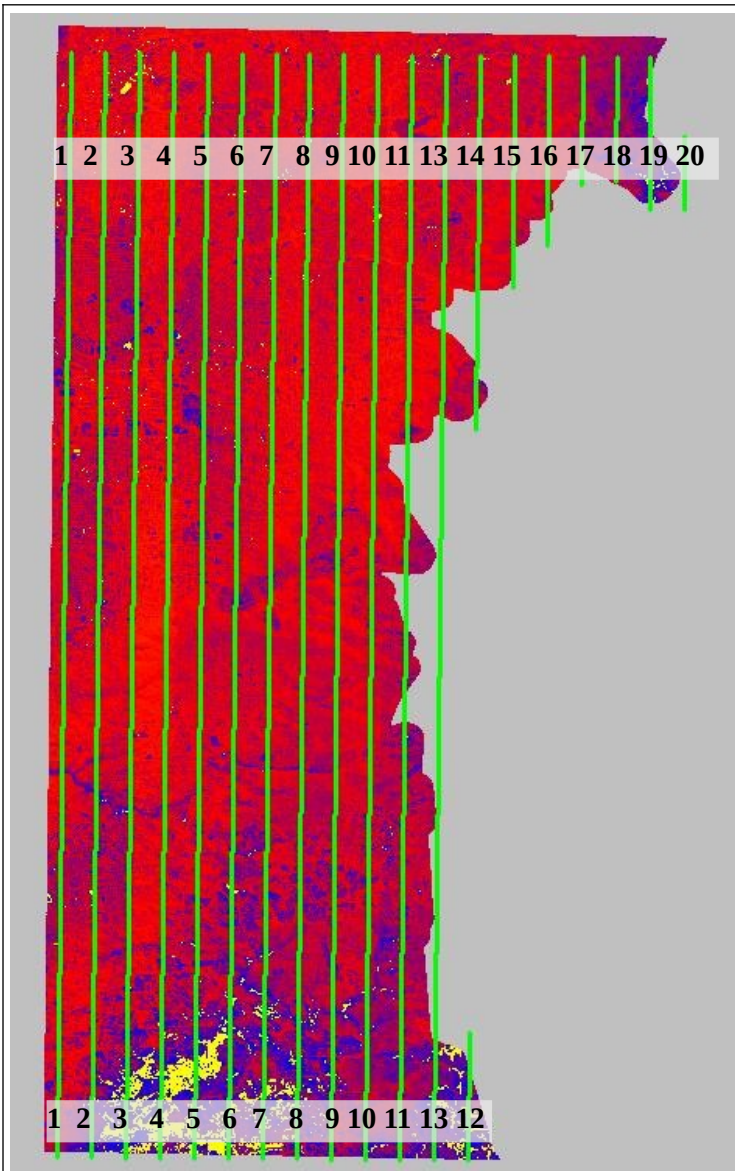| Line number	Mid-point time ACDT		Line number	Mid-point time ACDT
1	11:27		11	13:09
2	11:38		12	13:19
3	11:46		13	13:30
4	11:56		14	13:36
5	12:05		15	14:00
6	12:15		16	14:10
7	12:26		17	14:16
8	12:36		18	14:21
9	12:47		19	14:29
10	12:57		20	14:33
			21	14:36

North-East nighttime (220326, continuing into the following morning) flight line timing

Line number	Mid-point time ACDT		Line number	Mid-point time ACDT
1	23:30		11	01:28
2	23:42		12	01:41
3	23:50		13	01:51
4	00:02		14	02:00
5	00:10		15	02:09
6	00:23		16	02:18
7	00:33		17	02:26
8	00:52		18	02:35
9	01:03		19	02:38
10	01:16		20	02:43
			21	02:46
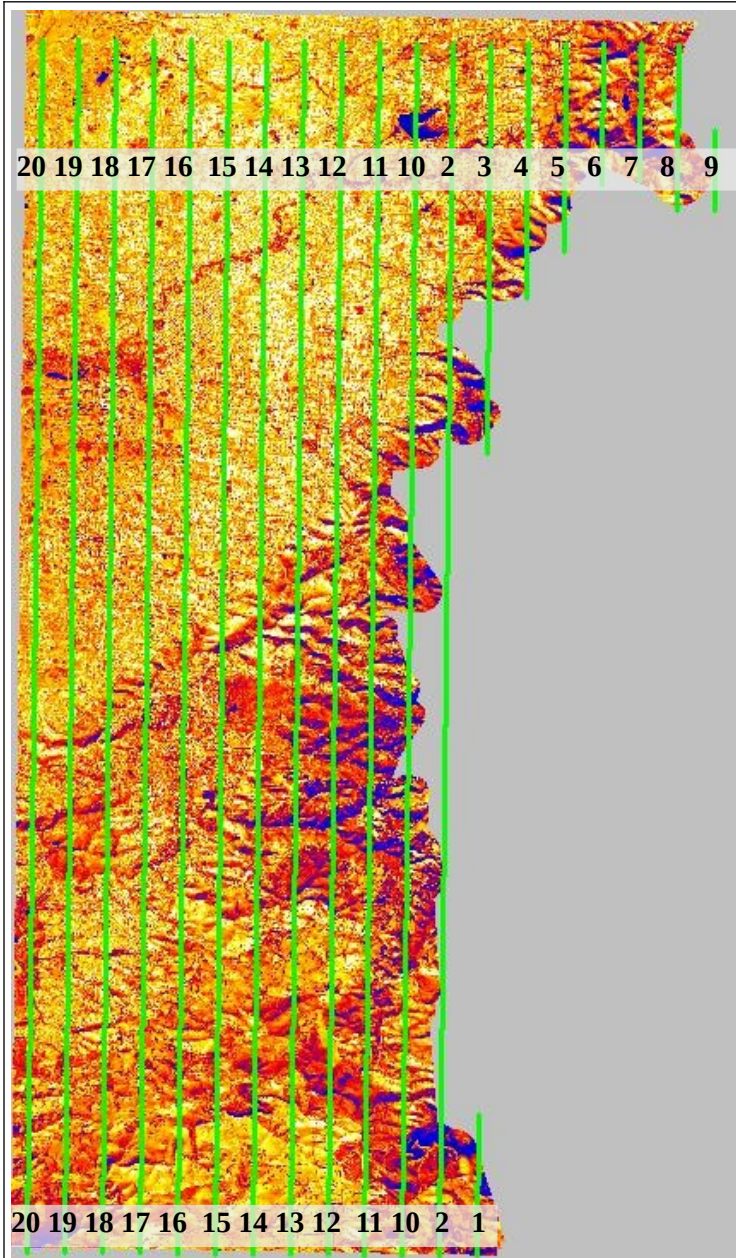
Centre-East daytime (220416) flight line timing

Line number	Mid-point time ACDT
1	12:08
2	12:20
3	12:30
4	12:36
5	12:40
6	12:43
7	12:47
8	12:50
9	12:53
10	13:06
11	13:23
12	13:37
13	13:50
14	14:04
15	14:19
16	14:33
17	14:46
18	15:00
19	15:17
20	15:32

Centre-East nighttime (220416, continuing into the following morning) flight line timing

Line number	Mid-point time ACDT
1	12:08
2	12:20
3	12:30
4	12:36
5	12:40
6	12:43
7	12:47
8	12:50
9	12:53
10	13:06
11	13:23
12	13:37
13	13:50
14	14:04
15	14:19
16	14:33
17	14:46
18	15:00
19	15:17
20	15:32

Data validation and context

As described above, thermal imagery data was collected across four days with combined daytime/nighttime flights on the 18th, 19th, 26th of March and the 16th of April 2022.
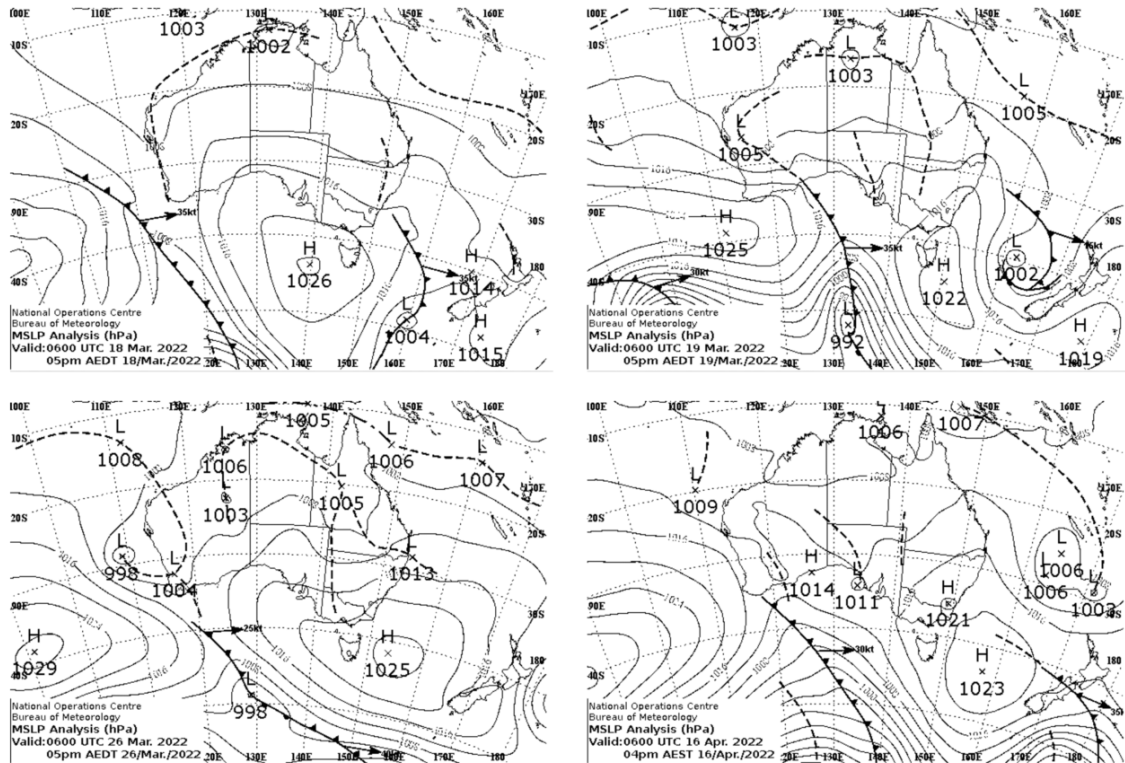
Synoptic situation

Illustration 4: Synoptic charts for 16:30 ACDT, 18th (top left), 19th (top right), and 26th (bottom left) of March 2022 and 16th (bottom right) of April 2022. Australian Bureau of Meteorology, 2022.

Each of these days displays a high pressure system to the south-east which results in weak northerlies to north-easterlies, ideal conditions for the development of an urban heat island.

Comparison data

Several data sources were identified to compare and validate the surface temperature measurements from the airborne thermal imagery. There are several BoM automatic weather stations in the study area, which provide time series of air temperature measurements as well as other meteorological parameters. This data is assimilated into the operational forecasting and analysis models to provide high resolution (12km) air temperature analyses (http://www.bom.gov.au/nwp/doc/access/NWPData.shtml). We note that air temperature is not expected to be a close match to the surface temperature although some degree of interrelation is anticipated.

More directly comparable datasets are independent radiometric measurements of surface temperature, and two satellite-based instrument products have been used to investigate correlation with the ARA airborne data: MODIS (Moderate Resolution Imaging Spectroradiometer), flown on NASA's Terra and Aqua flagship earth-observing satellites and providing a daily surface temperature product on a 1000m grid, and ECOSTRESS (Ecosystem Spaceborne Thermal Radiometer Experiment on Space Station), a thermal imager carried on the International Space Station, providing a much higher resolution (70m) surface temperature product although with less frequent, sun-asynchronous overpasses.

Australian Bureau of Meteorology Automatic Weather Stations

Five of the BoM's automatic weather stations (AWS) fall inside the study area, and their temperature measurements (in a Stevenson Screen, mounted 1.2m above ground) are shown below for the periods of all the flights covered by this report.

- 00: ADELAIDE (WEST TERRACE / NGAYIRDAPIRA)

  - latitude: -34.9257, longitude: 138.5832, height: 29.3 m

- 04: ADELAIDE AIRPORT

  - latitude: -34.9524, longitude: 138.5196, height: 2.0 m

- 07: PARAFIELD AIRPORT

  - latitude: -34.7977, longitude: 138.6281, height: 9.5 m

- 08: EDINBURGH RAAF

  - latitude: -34.7111, longitude: 138.6222, height: 16.5 m

- 10: NOARLUNGA

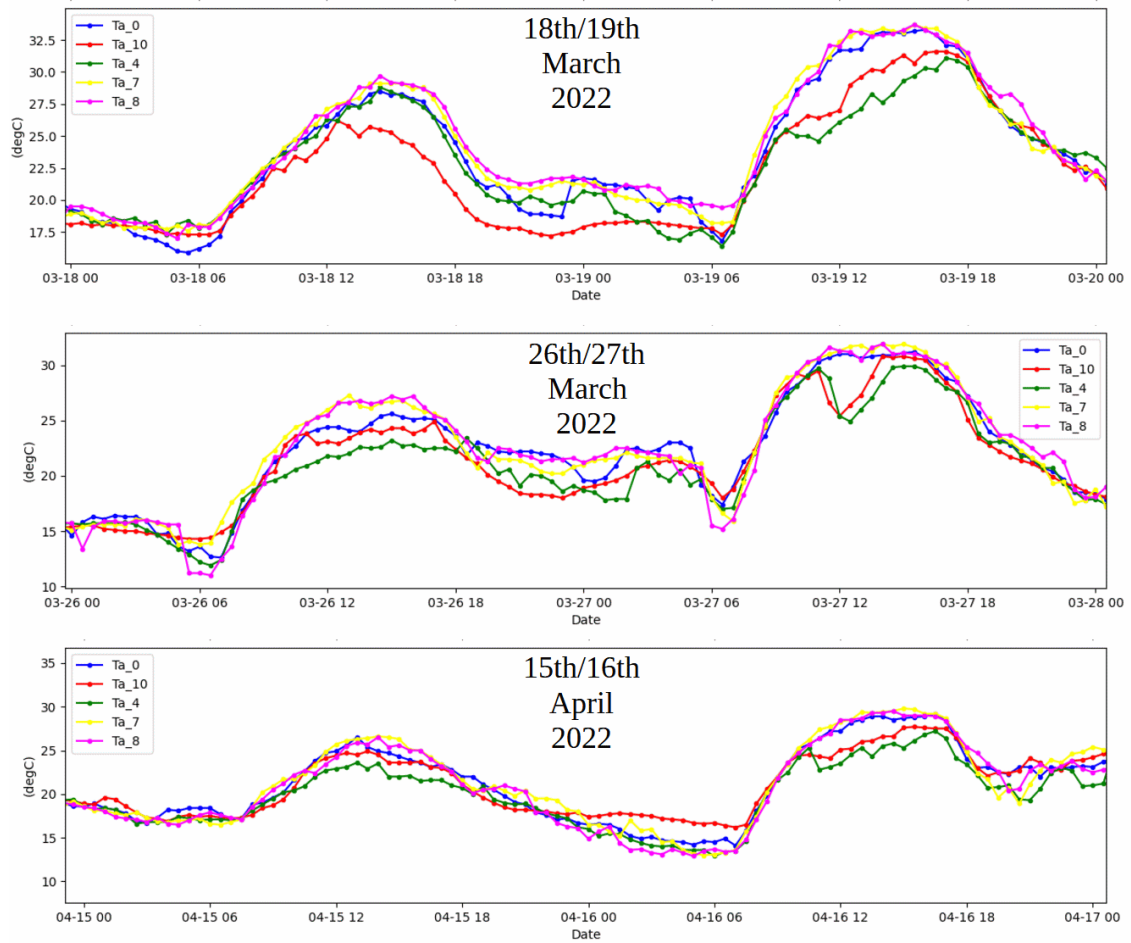 - latitude: -35.1586, longitude: 138.5057, height: 55.0 m

Illustration 5: Temperature records from Bureau of Meteorology automatic weather stations in degC. 0:ADELAIDE (WEST TERRACE / NGAYIRDAPIRA), 10:NOARLUNGA, 4:ADELAIDE AIRPORT, 7:PARAFIELD AIRPORT, and 8:EDINBURGH RAAF for the 18th and 19th of March 2022 (top), the 26th of March 2022 (centre) and the 16th of April 2022 (bottom).

Table 3: Average temperature in degC at the Bureau of Meteorology Automatic Weather Station site during flight time. The temperature is measured at 1.2 m above the ground, hence does not represent the same temperature as the surface skin temperature which is measured by the thermal infrared radiometric instruments (ARA's FLIR A615 thermal imager, MODIS and ECOSTRESS)

		Adl West Tce degC Ta_0	Noarlunga degC Ta_10	YPAD degC Ta_4	YPPF degC Ta_7	YPED degC Ta_8
Day	18/03/22	27.6	25.4	27.5	28.3	28.4
Night	18-19/03/2022	20.7	17.9	19.9	21.0	21.3
Day	19/03/22	32.5	29.7	27.6	33.0	32.9
Night	19-20/03/2022	21.6	21.5	22.6	21.5	22.0
Day	26/03/22	24.5	23.6	22.1	26.2	26.2
Night	26-27/03/2022	21.0	19.4	18.9	21.3	21.9
Day	16/04/22	28.4	26.3	25.0	29.1	28.8
Night	16-17/04/2022	24.1	24.9	23.4	24.7	22.7

Australian Bureau of Meteorology ACCESS-G Model output

As noted previously, the BoM assimilates data from its entire AWS network and other sources into the operational forecasting and analysis model ACCESS-G to provide high resolution (12km) air temperature analyses valid across the whole country (http://www.bom.gov.au/nwp/doc/access/NWPData.shtml). This provides air temperature data extending the area across which the AWS station measurements can be compared with other datasets.

The following pages show this air temperature analysis data relevant to all of this project's measurement flights, overlaid with the matching flight tracks.
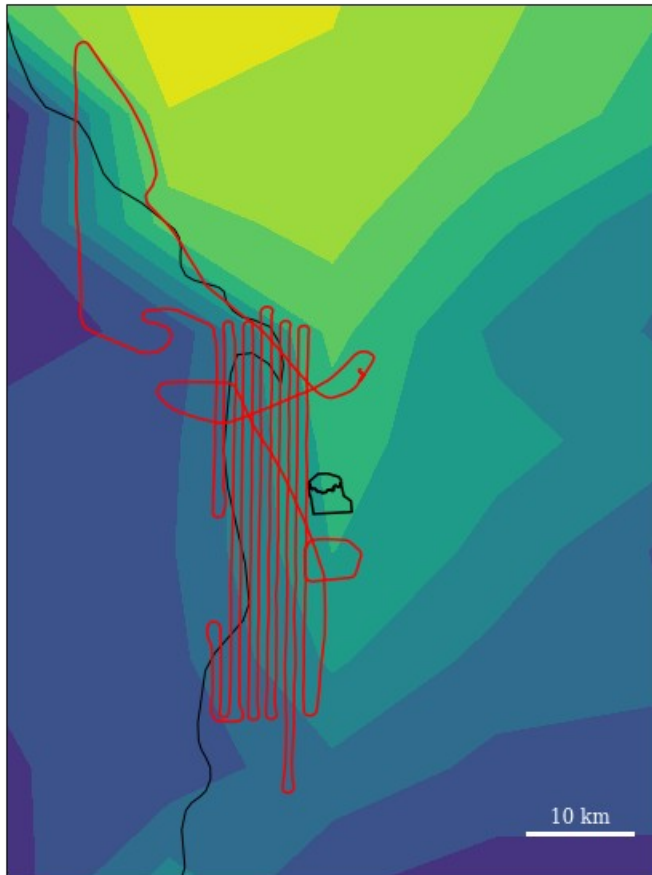
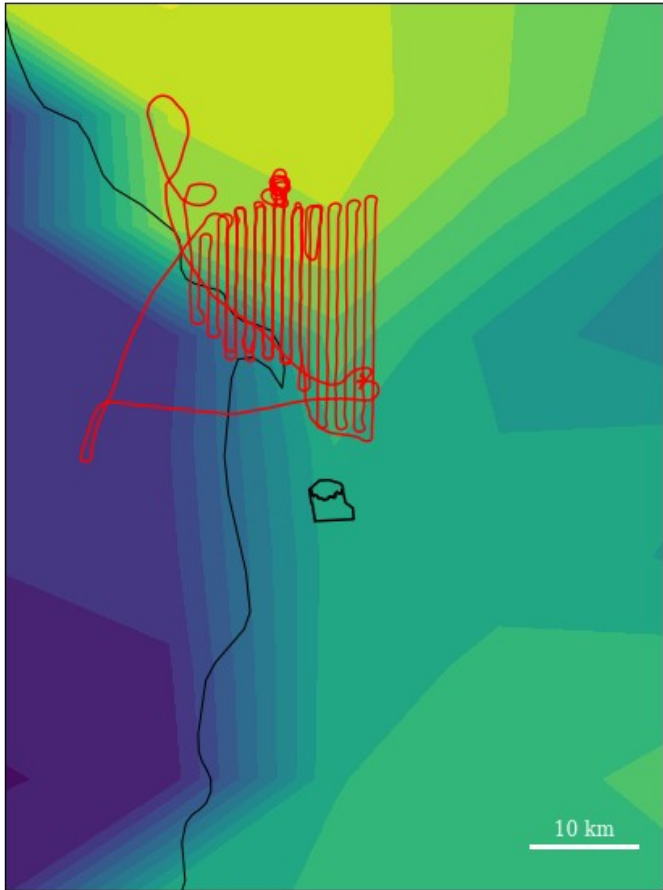**Day**

18/03/2022

03:00 UTC

13:30 ACDT

Night

19/03/2022

15:00 UTC

20/03/2022

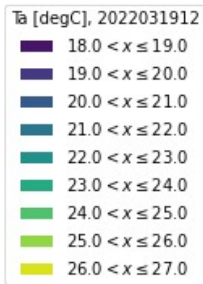01:30 ACDT
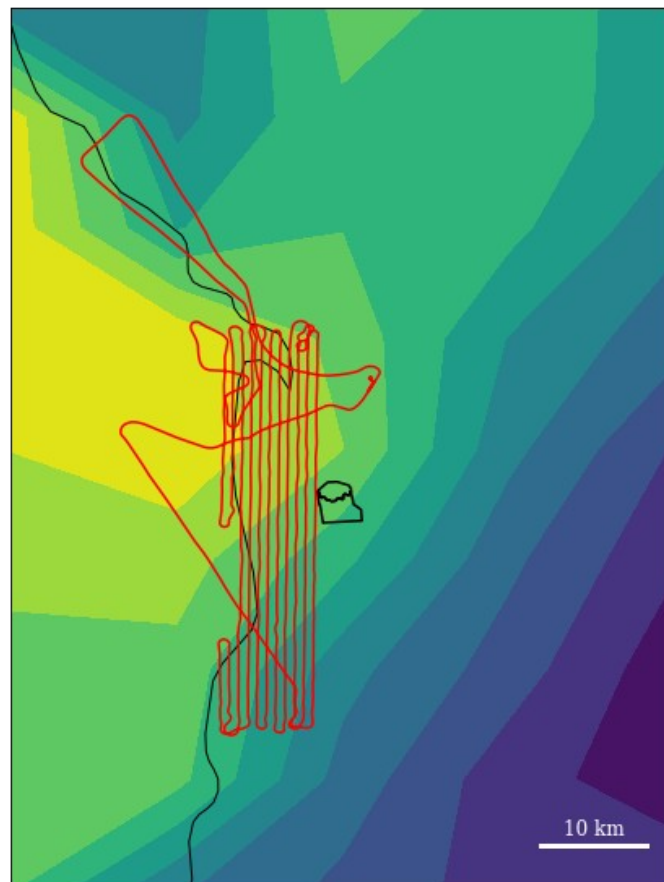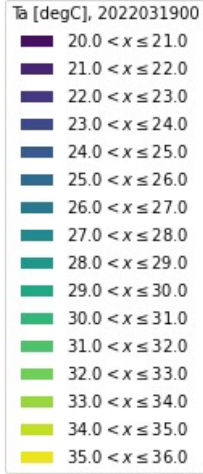
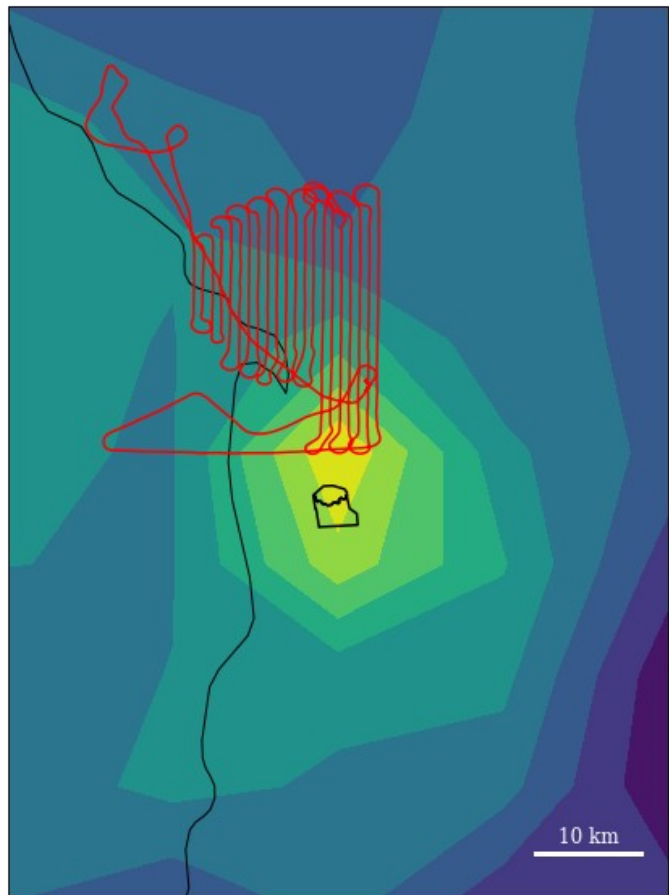**Day**

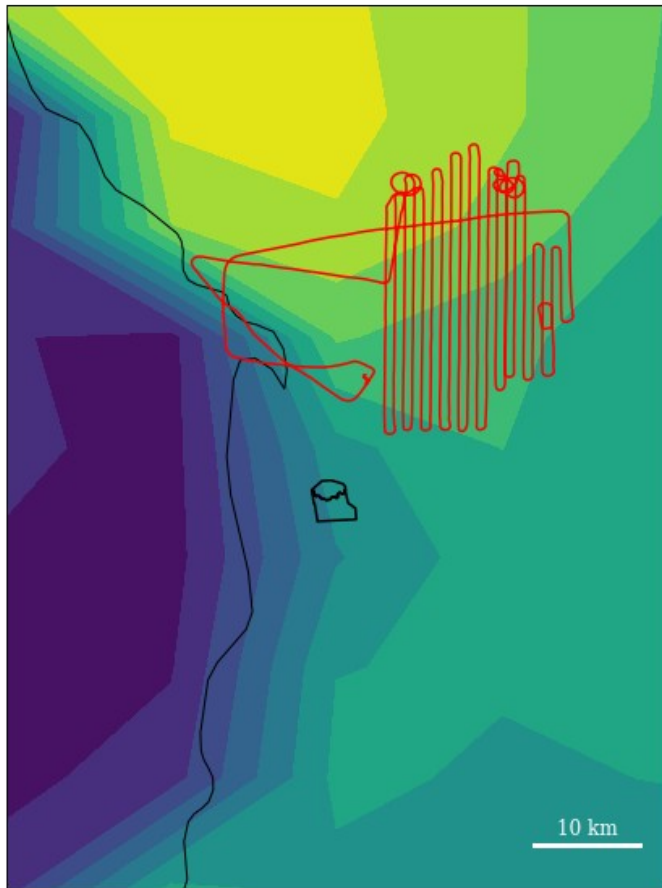19/03/2022

03:00 UTC

13:30 ACDT

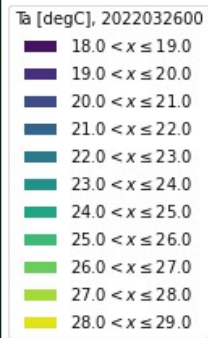**Night**

20/03/2022

15:00 UTC

21/03/2022

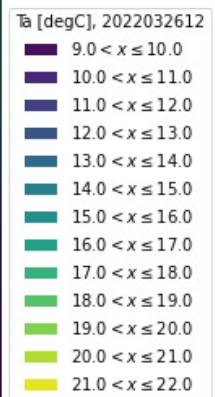01:30 ACDT

Day
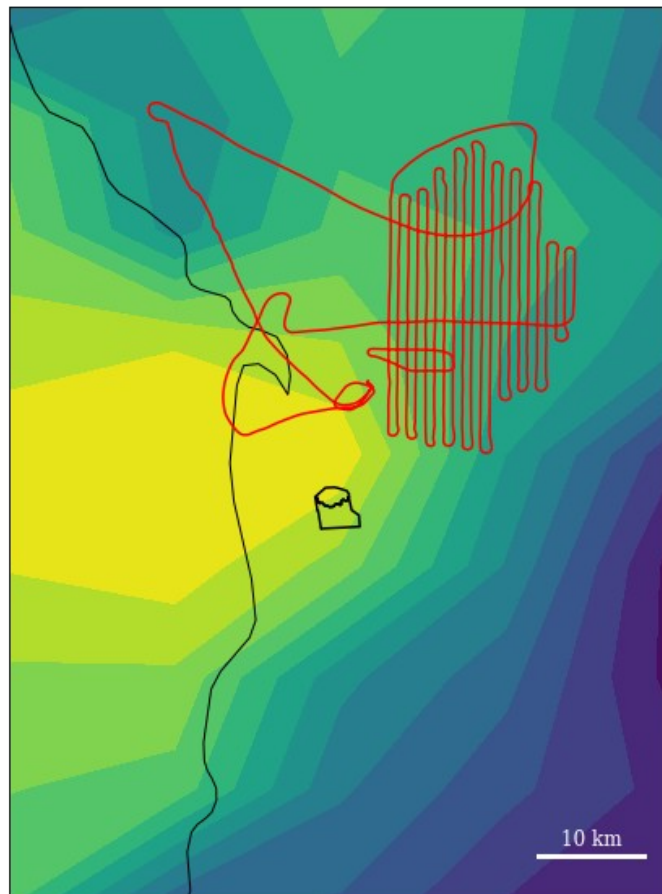
26/03/2022
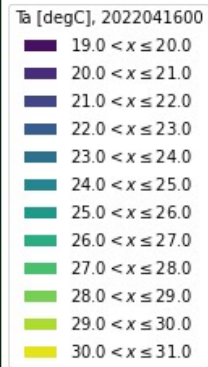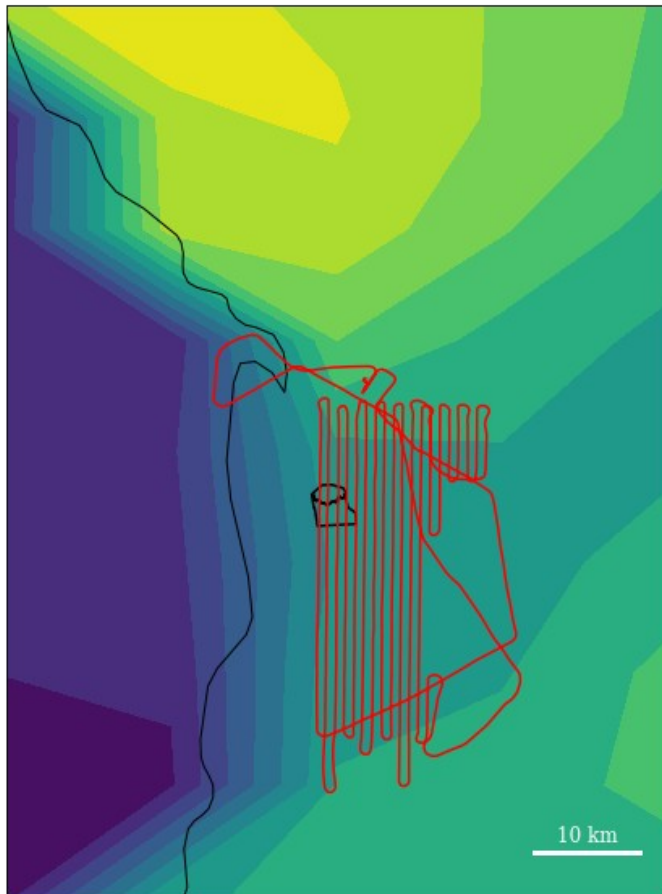
03:00 UTC

13:30 ACDT

Night

27/03/2022

15:00 UTC

28/03/2022

01:30 ACDT
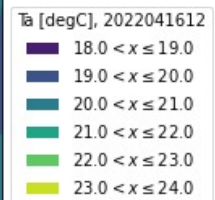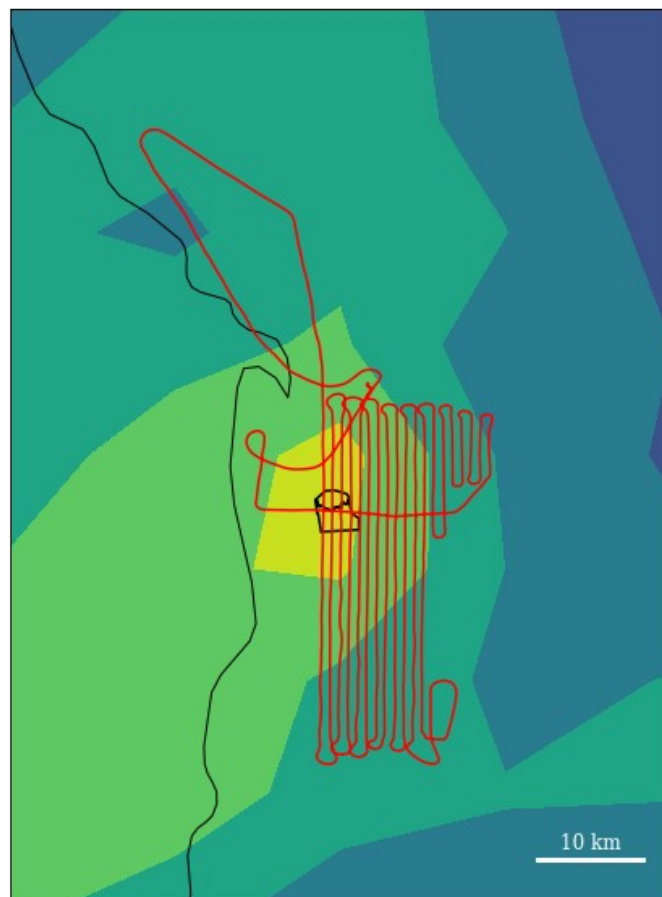
Day

16/04/2022

03:00 UTC

13:30 ACDT

Night

16/04/2022

15:00 UTC

17/04/2022

01:30 ACDT

Radiometric comparison datasets

Only limited direct comparison data is available with closely matching times of observation, however a significant and valuable assessment and validation exercise can be undertaken by comparison with various satellite-borne thermal imaging datasets. Different satellite have different overpass schedules and spatial resolution and so a survey was undertaken to identify suitable datasets for comparison with the airborne FLIR-615 imagery for this Adelaide UHI project.

Instrument	Scan Type	Platform	Number of TIR bands	Effective resolution	Effective revisit time
Advanced Very-High-Resolution Radiometer (AVHRR)	Conical scanning radiometer	POES / MetOp	4/6 [0.58 – 12.5] µm	[1.1 km (only for local area coverage, 10% of the time) – 3×4] km	1 day
MODIS	Cross-track scanning radiometer	Terra (EOS AM-1)	4 [3.660 - 4.080] µm	1 km	1 – 2 days
SLSTR	Conical scanning radiometer	Sentinel-3	9 [0.55 – 12] µm	500 m	Less than 2 days
TIRS	Pushbroom imager	Landsat 8-9	2 [10.60 – 12.51] µm	100 m	8 days
PhyTIR ECOSTRESS	Push-whisk scanning radiometer	International Space Station (ISS)	5 [8.29 – 12.09] µm	70 m	Approx. 3.5 days strongly dependent on ISS orbital operations

Based on these instrument characteristics, we conducted analyses comparing the FLIR imagery with the closest available land surface temperature products from MODIS (good temporal alignment with the airborne data although only at 1km spatial resolution) and ECOSTRESS (moderate temporal alignment but highest available spatial resolution).
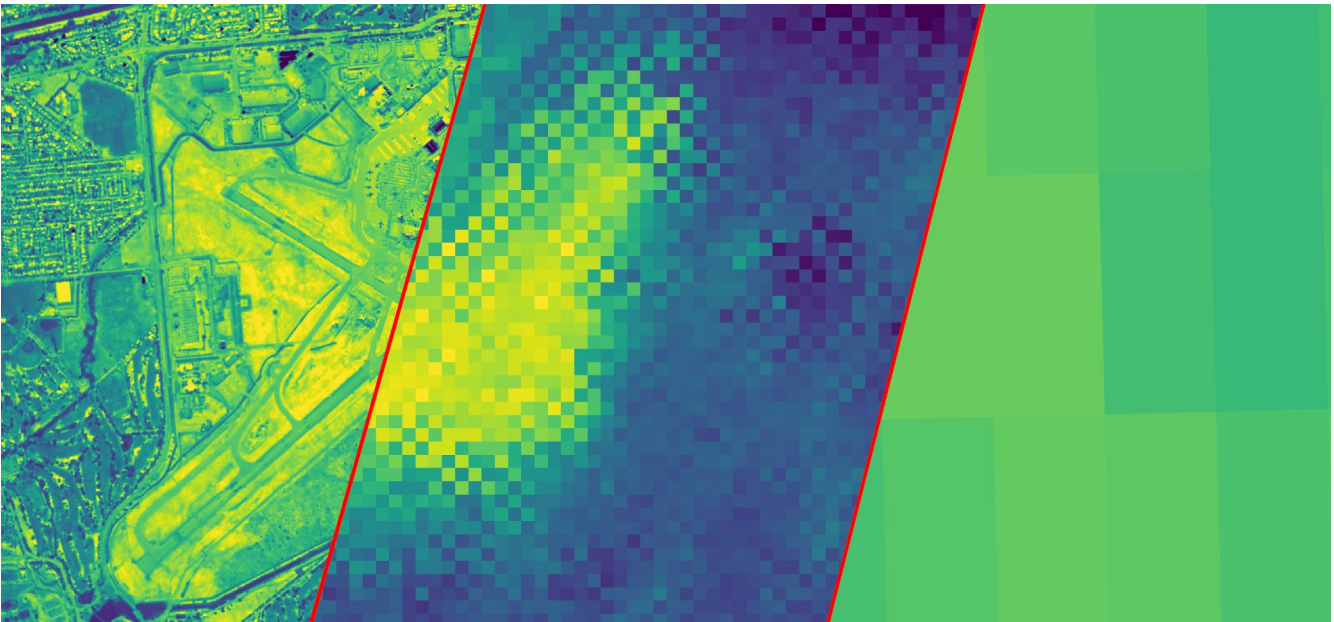
From left to right: FLIR A615 thermal imager, PhyTIR (ECOSTRESS), SLSTR (Sentinel-3).

Comparison with MODIS data

As noted previously, MODIS is an important instrument operated by NASA on its Terra and Aqua earth observing satellites, with daily sun-synchronous overpasses (https://modis.gsfc.nasa.gov/).

MOD11A1 is a tile of daily land surface temperature (LST) product at 1200 rows by 1200 columns, which gives a 1km spatial resolution and it is gridded in the sinusoidal projection. The exact grid size at 1 km spatial resolution is 0.928 km by 0.928 km. The algorithm used to construct the 1 km resolution daily LST is described in Wan (2013).

Wan, 2013: Collection-6 MODIS Land Surface Temperature Products Users' Guide. https://lpdaac.usgs.gov/documents/118/MOD11_User_Guide_V6.pdf [accessed: 22/09/2022]

The relevant MODIS overpasses were selected for comparison with the ARA-FLIR imagery from the NASA data by the Julian day of each ARA measurement flight, LST_Day_1km (MOD11A1.061) and LST_Night_1km (MOD11A1.061):

18th March 2022   = 077

19th March 2022   = 078

26th March 2022   = 085

16th April 2022   = 106

As an example, LST data from the first flight (18th of March, daytime) is shown below overlaid with both MODIS LST and ACCESS-G air temperature. Good agreement between datasets is apparent by eye in this overlay.
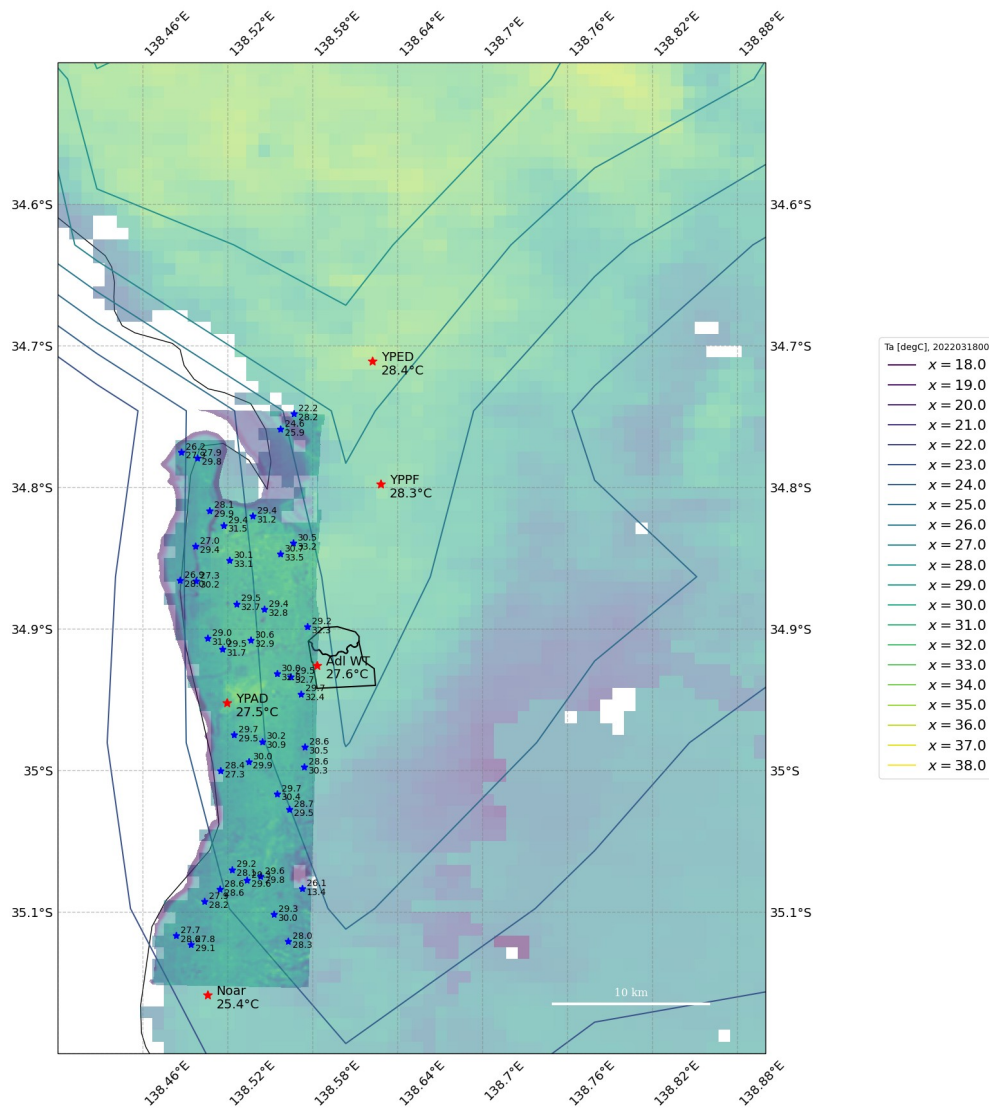
Illustration 6: ARA FLIR data layer over the Adelaide region over MODIS LST 1 km for 18th March 2022 day time, MODIS day 077. FLIR pixel data were averaged over 128 data points. Contours shown are ACCESS-G data forecast for the 2 m temperature, 2022031803. Red stars display the AWS sites with the average air temperature over the flight period, blue stars show a number of average temperature values in a circle of 1 km radius. The upper value is FLIR data, the low is MODIS. Data in deg C.

In order to meaningfully compare the data collected by this project with the much lower resolution MODIS imagery, a technique was adopted to form an average reported temperature across a circle of 1000m radius from the comparison point, for both datasets.

This comparison was done for each available AWS location (shown in the table below)

as well as across a large number of points along the flight track, shown in the scatter plots. Note that with only a small number of MODIS sample points contributing to this average, stochastic noise will necessarily be significant and the scatter plots are considered to be more representative than any indvidual point comparison, because these are based on a large ensemble of comparisons.

Table 4: MODIS and ARA-FLIR average temperatures over a radius of 1000 m centred around the AWS location (blank cells indicate no data available). The flights on 26/03/2022 and 16/04/2022 did not cover any AWS.

		Adl West Tce degC Ta_0	Noarlunga degC Ta_10	YPAD degC Ta_4	YPPF degC Ta_7	YPED degC Ta_8	
Day	18/03/22	31.5	30.0	31.2	32.4	34.7	MODIS
				30.6			FLIR
		27.6	25.4	27.5	28.3	28.4	AWS
Night	18-19/03/2022	19.5	16.1	18.2	20.0	20.3	MODIS
				15.7			FLIR
		20.7	17.9	19.9	21.0	21.3	AWS
Day	19/03/22						MODIS
					29.2	33.7	FLIR
		32.5	29.7	27.6	33.0	32.9	AWS
Night	19-20/03/2022	22.4	20.6	21.4	17.1	22.2	MODIS
					16.8	17.8	FLIR
		21.6	21.5	22.6	21.5	22.0	AWS
Day	26/03/22		25.0	15.0	28.2	29.6	MODIS
							FLIR
		24.5	23.6	22.1	26.2	26.2	AWS
Night	26-27/03/2022	18.3	16.6	14.6	18.3	18.7	MODIS
							FLIR
		21.0	19.4	18.9	21.3	21.9	AWS
Day	16/04/22	27.6	27.2	26.9	29.7	29.6	MODIS
							FLIR
		28.4	26.3	25.0	29.1	28.8	AWS
Night	16-17/04/2022	13.9	18.4	16.1	20.1	19.0	MODIS
							FLIR
		24.1	24.9	23.4	24.7	22.7	AWS

f(x) = 0.9 x + 4.3
R^2 = 0.6
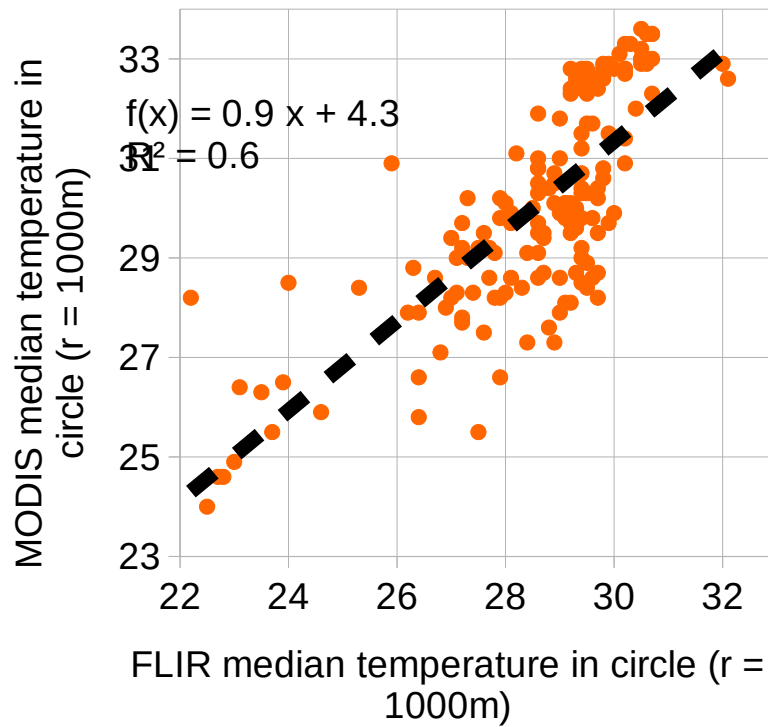
Illustration 7: 18 March 2022, day: Comparison between ARA-FLIR measurements and MODIS at locations along the ARA flight track. The median temperature is calculated in a circle around the track location of a 1000m radius for the FLIR and MODIS data. Note, MODIS data has a resolution approximately of 1 km by 1km, hence only a limited number of data points will result in the MODIS data circle median (between 4 and 5 data points), while the FLIR median temperature is calculated from about 0.9×10^6 data points. Data points close to the coastline were removed from this analysis to avoid related bias.

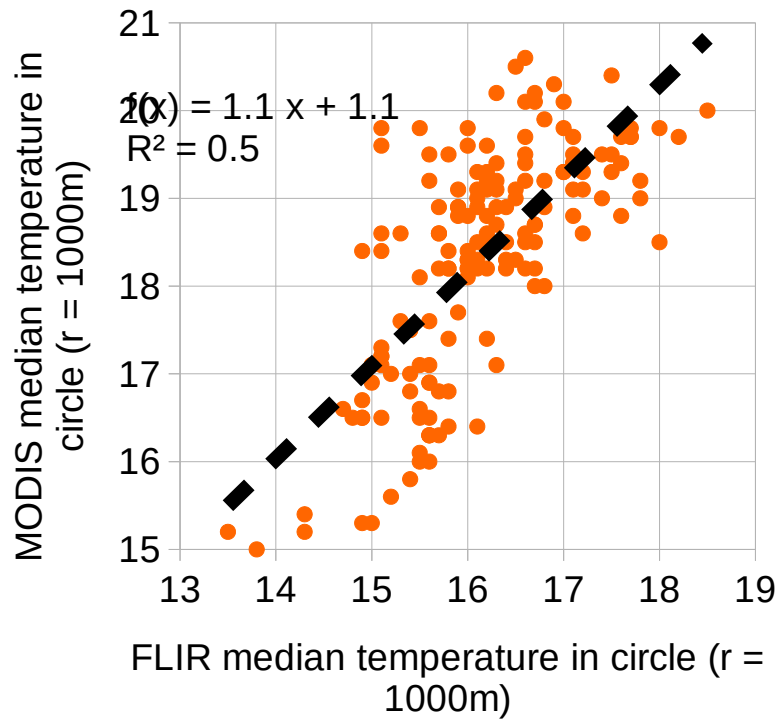*Illustration 8: 18 March 2022, night: Comparison at lat/lon values along the ARA flight track. Same as Illustration 7 but for nighttime.*

High resolution comparison: ECOSTRESS thermal imagery

Apart from its higher spatial resolution (70m), ECOSTRESS data enables application of the well-established Temperature and Emissivity Separation algorithm (TES) and derivation of a comprehensive land cover spectral library. This provides an effective emissivity corrected-land surface temperature product not possible with with data from a single-band measurement from a microbolometer array such as used in the FLIR-A615 instrument or similar, most commonly used for airborne thermal imaging surveys. See https://ecostress.jpl.nasa.gov/downloads/psd/ECOSTRESS_SDS_PSD_L2_ver1-1.pdf for more detail.

Firstly, a survey was undertaken to identify the most suitable ECOSTRESS overpass for analysis. The unusually moist and persistent La Nina-dominated weather situation that led to problems in finding suitable conditions for the day/night combination discussed earlier also affects the search for suitable satellite data. Approximately 70 potential datasets were inspected and data granules with high cloud coverage above the area were discarded in absence of an accurate cloud cover filter. The closest matching suitable data was found to be from a coincident overpass on 19th March at 09:30 (local time), 9 hours after the most closely matching flight of the night of the 18th,was available for direct comparison. No other images free from cloud during the period covered by the flights were found.

 The closest overpass used for direct comparisons was:

ECOSTRESS_L2_LSTE_20972_013_20220318T211447_0601_01

In order to directly compare data with the FLIR mosaics, Level-2 ECOSTRESS Land Surface Temperature and Emissivity was reprojected into coordinate system WGS 84 / UTM zone 54S (EPSG:32754) using Level-1B Geolocation data. These are derived primarily from the ISS orbital parameters. Propagated errors from this measurement are estimated to be 2.5 km at 1-σ (Level-1B Resampling and Geolocation Algorithm Theoretical Basis Document (ATBD), JPL D-94641).

Fine coregistration was then achieved by matching the scene with LandSat orthorectified imagery. This process could not be used for nighttime observations and images with cloudy areas near the terminator. Such cases were manually georeferenced when possible without further geometrical control to achieve an estimated 100 – 200 m geometric accuracy (two to three ECOSTRESS pixels).

Plotting average temperatures from this "best pass" ECOSTRESS data sampled to the area covered by the four nearest airborne FLIR measurement flights study area against the average derived from those flight data, we form a "pseudo timeseries" that shows the data to be at least consistent across the measurement types (Illustration 9).
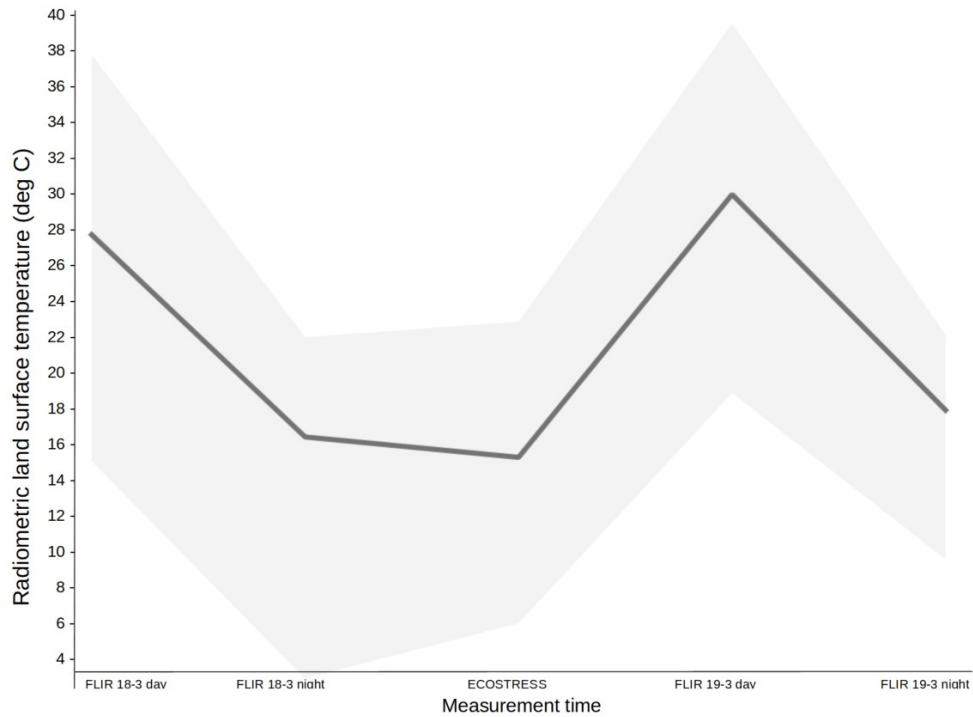

Illustration 9: Land Surface Temperature pseudo-time series built upon data gathered around 22/03/18-13:00, 22/03/19 00:00, 22/03/19-09:30 (ECOSTRESS), 22/03/19-13:00 and 22/03/19-00:15. Mean and range are shown.

This comparison is further broken down by land use, filtered using publicly available SA Government land use classification data (SA Land Cover Layers 1987 – 2015, https://data.sa.gov.au/data/dataset/sa-land-cover/resource/c856ebe3-f9bc-4ea8-ac3b-7e2cc877fea3). The analysis shown in Illustration 10 highlights differences in the diurnal cycle related to differences in emissivity, specific heat, shape, etc. High specific heat of water bodies (class 17) or expected high variability of dryland agriculture (class 8) can be identified.

| 1 Woody Native Vegetation	10 Irrigated Non-Woody
2 Mangrove Vegetation	11 Orchards/ Vineyards
3 Non-Woody Native Vegetation	12 Plantation (Softwood)
4 Saltmarsh Vegetation	13 Plantation (Hardwood)
5 Wetland Vegetation	14 Urban Area
6 Natural Low Cover	15 Built-up Area
7 Salt Lake/ Saltpan	16 Disturbed Ground / Outcrop
8 Dryland Agriculture	17 Water Unspecified
9 Exotic Vegetation	18 No Data/ Unclassified
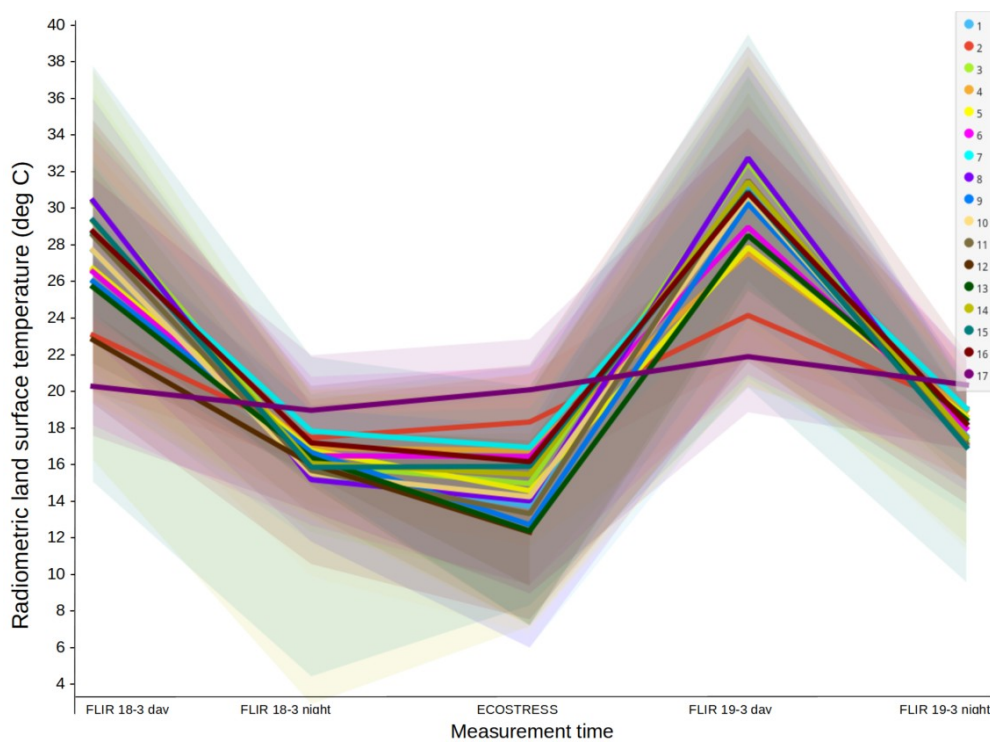
Illustration 10: Pseudo-timeseries similar to Illustration 9 but broken down by land use classification.

For a direct statistical comparison, FLIR A615 data were downsampled to a resolution matching the ECOSTRESS data of 70 m by using an area-weighted mean value.

Table 5: Correlation matrix for a range of statistical comparison measures, comparing ECOSTRESS measurements with the four nearest airborne FLIR measurements downsampled to a matching spatial resolution.

		FLIR, 18-Mar day time	FLIR, 18-Mar night time	ECOSTRESS	FLIR, 19-Mar day time	FLIR, 19-Mar night time
FLIR, 18-Mar day time	Pearson's r	—				
	p-value	—				
	Spearman's rho	—				
	p-value	—				
FLIR, 18-Mar night time	Pearson's r	-0.463	—			
	p-value	< .001	—			
	Spearman's rho	-0.278	—			
	p-value	< .001	—			
ECOSTRESS_LST_220318 T211447	Pearson's r	**-0.694**	**0.704**	—		
	p-value	**< .001**	**< .001**	—		
	Spearman's rho	**-0.423**	**0.661**	—		
	p-value	**< .001**	**< .001**	—		
FLIR, 19-Mar day time	Pearson's r	0.978	-0.828	**-0.686**	—	
	p-value	< .001	< .001	**< .001**	—	
	Spearman's rho	0.964	-0.748	**-0.405**	—	
	p-value	< .001	< .001	**< .001**	—	
FLIR, 19-Mar night time	Pearson's r	-0.570	0.815	**0.686**	-0.708	—
	p-value	< .001	< .001	**< .001**	< .001	—
	Spearman's rho	-0.536	0.839	**0.524**	-0.536	—
	p-value	< .001	< .001	**< .001**	< .001	—

Note that a strong correlation was found between the ECOSTRESS data and the most closely timewise matching FLIR dataset, from the nighttime of the 18th of March. This agreement indicates that the FLIR data is an accurate representation of the physical reality. Full details of the statistical comparison are provided in Appendix 4.

Appendices

Appendix 1 – Datasheet of FLIR A615 Thermal Imager

FLIR A315 / A615 Technical Specifications

Camera specific

Imaging and optical data

	FLIR A315	FLIR A615
Spatial resolution (IFOV)	1.36 mrad	0.69 mrad
Focal length	18 mm	24.5 mm
F-number	1.3	1.0
Image frequency	60 Hz	50 Hz (100/200 Hz with windowing)

Detector data

	FLIR A315	FLIR A615
IR resolution	320 × 240 pixels	640 × 480 pixels
Detector pitch	25 μm	17 μm
Detector time constant	Typical 12 ms	Typical 8 ms

Measurement

	FLIR A315	FLIR A615
Object temperature range	−20 to +120°C 0 to +350°C	-20 to +150°C +100 to +650°C +300 to +2000°C

USB

	FLIR A315	FLIR A615
USB	N/A	Control and image
USB, standard	N/A	USB 2 HS
USB, connector type	N/A	USB Mini-B
USB, communication	N/A	TCP/IP socket-based FLIR proprietary
USB, image streaming	N/A	16-bit 640 × 480 pixels at 25 Hz 16-bit 640 × 240 pixels at 50 Hz 16-bit 640 × 120 pixels at 100 Hz - Signal linear - Temperature linear - Radiometric
USB, protocols	N/A	TCP, UDP, SNTP, RTSP, RTP, HTTP, ICMP, IGMP, ftp, SMTP, SMB (CIFS), DHCP, MDNS (Bonjour), uPnP

Measurement analysis

Atmospheric transmission correction	Automatic, based on inputs for distance, atmospheric temperature and relative humidity
Optics transmission correction	Automatic, based on signals from internal sensors
Emissivity correction	Variable from 0.01 to 1.0
Reflected apparent temperature correction	Automatic, based on input of reflected temperature
External optics/windows correction	Automatic, based on input of optics/window transmission and temperature
Measurement corrections	Global object parameters

Ethernet

Ethernet	Control and image
Ethernet, standard	IEEE 802.3
Ethernet, connector type	RJ-45
Ethernet, type	Gigabit Ethernet
Ethernet, communication	TCP/IP socket-based FLIR proprietary and GenICam protocol
Ethernet, protocols	TCP, UDP, SNTP, RTSP, RTP, HTTP, ICMP, IGMP, ftp, SMTP, SMB (CIFS), DHCP, MDNS (Bonjour), uPnP

Digital input/output

Digital input	2 opto-isolated, 10–30 VDC
Digital output, purpose	Output to ext. device (programmatically set)
Digital output	2 opto-isolated, 10–30 VDC, max 100 mA
Digital I/O, isolation voltage	500 VRMS
Digital I/O, supply voltage	12/24 VDC, max 200 mA
Digital I/O, connector type	6-pole jackable screw terminal
Digital input, purpose	Image tag (start, stop, general), Image flow ctrl. (Stream on/off), Input ext. device (programmatically read)

Power system

External power operation	12/24 VDC, 24 W absolute max
External power, connector type	2-pole jackable screw terminal
Voltage	Allowed range 10–30 VDC

Digital input/output

Digital input, purpose	Image tag (start, stop, general), Image flow ctrl. (Stream on/off), Input ext. device (programmatically read)

Ethernet

Ethernet, image streaming	16-bit 320 × 240 pixels at 60 Hz - Signal linear - Temperature linear - Radiometric GigE Vision and GenlCam compatible	16-bit 640 × 480 pixels at 50 Hz 16-bit 640 × 240 pixels at 100 Hz 16-bit 640 × 120 pixels at 200 Hz - Signal linear - Temperature linear - Radiometric GigE Vision and GenlCam compatible

	FLIR A315 - Standard	FLIR A315f - Environmental housing	FLIR A615 - Standard
Environmental data			
Operating temperature range	−15°C to +50°C	−25°C to +50°C	−15°C to +50°C
Encapsulation	IP 40 (IEC 60529)	IP 66 (IEC 60529)	IP 40 (IEC 60529)
Bump	25 g (IEC 60068-2-29)	5 g, 11 ms (IEC 60068-2-27)	25 g (IEC 60068-2-29)

Physical data			
Weight	0.7 kg	5 kg	0.9 kg
Camera size (L × W × H)	170 × 70 × 70 mm	460 × 140 × 150 mm	216 x 73 x 75 mm
Tripod mounting	UNC ¼"-20 (on three sides)	N/A	UNC ¼"-20 (on three sides)
Base mounting	2 × M4 thread mounting holes (on three sides)	TBA	2 × M4 thread mounting holes (on three sides)

System features			
Automatic heaters	N/A	Clears ice from window	N/A

General

Imaging and optical data

Field of view (FOV) / Minimum focus distance	25° × 18.8° / 0.4 m
Lens identification	Automatic
Thermal sensitivity/NETD	< 0.05°C @ +30°C / 50 mK
Focus	Automatic or manual (built in motor)

Detector data

Focal Plane Array (FPA) / Spectral range	Uncooled microbolometer / 7.5–13 µm

Measurement

Accuracy	±2°C or ±2% of reading

Environmental data

Storage temperature range	−40°C to +70°C
Humidity (operating and storage)	IEC 60068-2-30/24 h 95% relative humidity +25°C to +40°C
EMC	• EN 61000-6-2:2001 (Immunity) • EN 61000-6-3:2001 (Emission) • FCC 47 CFR Part 15 Class B (Emission)
Vibration	2 g (IEC 60068-2-6)

Physical data

Housing material	Aluminium

Scope of delivery

Hard transport case or cardboard box, Infrared camera with lens, Utility CD-ROM, Calibration certificate, Ethernet™ cable, USB cable (FLIR A615), Mains cable, Power cable (pig-tailed), Power supply, Printed Getting Started Guide, Printed Important Information Guide, User documentation CD-ROM, Warranty extension card or Registration card, 6-pole screw terminal (mounted on camera)

Appendix 2 Hyperspectral linescanner specifications

Separate PDF file attached – AisaEAGLE_datasheet_ver2-2012.pdf

Appendix 3 OxTS RT4003 IMU specifications

Separate PDF file attached – AisaEAGLE_datasheet_ver2-2012.pdf

Appendix 4 Detailed statistical comparison with ECOSTRESS, independent space-based radiometric thermography

A strong correlation was found between ECOSTRESS_LST_220318T211447 and the FLIR data from the preceding night, 220318n.

Point-to-point comparisons vary, but this is expected due to the differences in the diurnal cycle as seen in the pseudo-time series plots. This is seen in the per-land class residuals plots below, which show histograms of point-to-point differences between FLIR and ECOSTRESS.

The purpose of this analysis is not to demonstrate a perfect agreement, something unfeasible at this stage due to the time differences between observations, but to investigate limitations in the direct interpretation of these results.

The negative correlation with diurnal temperatures suggests hysteresis in these temperatures (unsurprisingly), governed to some extent by differences in emissivity and specific heat capacity, and possibly spatial structure.

For this particular pair, the residuals after substracting the mean difference between both observations (water bodies filtered out), were found to be:

	Residuals
Mean (before zeroed)	-0.386
Standard deviation	1.33
Minimum	-23.2
Maximum	15.2
50th percentile (absolute value)	0.799
75th percentile (absolute value)	1.38
95th percentile (absolute value)	2.51

Residuals are plotted against land cover class in the figure (right).

Linear regression for each class is plotted along with with standard error on the next page, suggesting a strong dependence on thermal properties of the land cover class.

Correlation, as expected, strongly depends on time between observations.
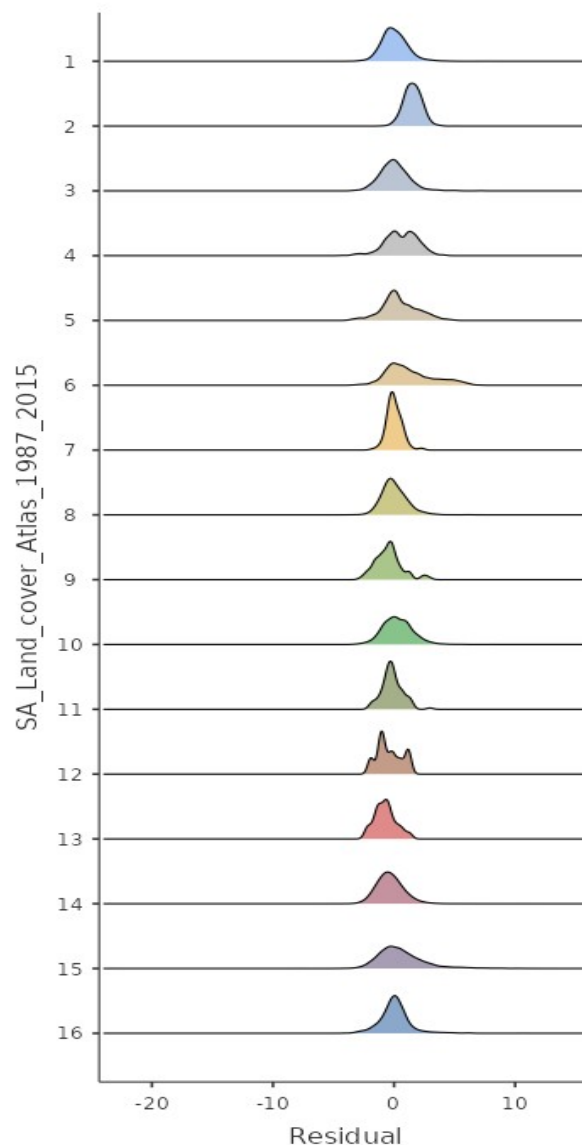
A scatter plot shows point-to-point comparison between FLIR and ECOSRTRESS.